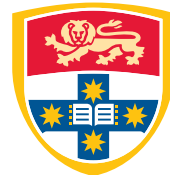

Investigation of The Aerodynamic Characteristics of Propeller Interactions for Mini Aerial Vehicles

Jasmine Warner

Supervisors: Prof. Dries Verstraete



THE UNIVERSITY OF
SYDNEY

School of Aerospace, Mechanical and Mechatronic Engineering

The University of Sydney

A thesis submitted to The University of Sydney in fulfilment of the requirements for
the degree of *Bachelor of Engineering Honours*

Jan 2022

[Dedication]

Declaration

I, Jasmine Warner, hereby declare that this thesis submission titled *Aerodynamic Characteristics of a Generic Micro-Aerial Vehicle to Investigate Propeller Interactions* is my own work and that, to the best of my knowledge and belief, it contains no material previously published or written by another person nor material which to a substantial extent has been accepted for the award of any other degree or diploma of the University or other institute of higher learning, except where due acknowledgement has been made in the text. Specifically, the work I contributed consists of:

1. Conducting the literature review
2. Assisting in producing a 3D model of the generic micro aerial vechicle
3. Wind tunnel testing of the generic micro aerial vechicle model
4. Analysing data of wind tunnel results; and
5. Writing this thesis report.

Assistance was received from my supervisor in the areas of:

1. Distinguishing relevant literature in respect to this thesis
2. Indicating critical software required; and
3. Ameliorating this thesis through constant feedback.

Jasmine Warner

Author

Date

Prof. Dries Verstraete

Supervisor

Date

Acknowledgements

Investigation of The Aerodynamic Characteristics of Propeller Interactions for Mini Aerial Vehicles

Abstract

Micro Aerial Vehicles (MAVs) are a class of unmanned aerial vehicles that are much smaller in size. These small aircraft allow for the observation of hazardous environments which are inaccessible to ground vehicles. Due to their small size they are much more difficult to design and manufacture. The additional complexity is due to several main factors including: low speed flight, small physical dimensions, structural strength, reduced stall speed and low inertia. With MAV design becoming one of the fastest-growing areas of development in the aerospace industry, there is an increasing need to have accurate experimental data to validate, simulate and model varieties of MAV configurations. One of the core but currently missing investigations is into the influence of effect of propellers on the aerodynamics and stability of MAV's

Executive Summary

Todo list

interrogate Ben	47
finish + add photo	48
add figure here	48
abb	48
finsiht this	49
right word?	52
fix the fig to Figure	56
change line style here	58
get rid of extra no prop lines - keep one only	59
cite	79
change this to a cite	80

Table of contents

List of figures	xvii
List of tables	xxi
List of abbreviations	xxii
Glossary	xxiii
1 Introduction	1
1.1 Problem Statement	3
1.2 Objectives	4
1.3 Outline	4
2 Background	6
2.1 Aircraft Geometry	6
2.2 Span	7
2.3 Chord	7
2.4 Sweep	8

Table of contents

2.5 Dihedral	10
2.6 Twist and Incidence	11
2.7 Aspect Ratio	12
2.8 Reference Frames	13
2.9 Earth Centered Axes: denoted as (x_e, y_e, z_e)	14
2.10 LVLH Axes: denoted as (x_v, y_v, z_v)	15
2.11 Body Axes: denoted as (x_b, y_b, z_b)	15
2.12 Stability Axes: denoted as (x_s, y_s, z_s)	16
2.13 Air Path Axes: denoted as (x_a, y_a, z_a)	16
2.14 Key Parameters	16
2.15 Aerodynamic Forces and Coefficients	17
2.16 Static Longitudinal Stability	19
2.17 Static Lateral Stability	22
2.18 Reynolds Number	24
3 Literature Review	27
3.1 Proliferation of MAV's in the Aerospace Landscape	27
3.2 Limitations of MAV Design Techniques	28

Table of contents

3.3 Low Reynolds Number Effects	29
3.3.1 Laminar Separation Bubbles and Vortices	33
3.3.2 Non-Linear Lift Distribution	37
3.4 Propeller Wing Interaction	38
3.4.1 Stability Effects	43
3.4.2 Aerodynamic Parameters	44
3.4.3 The General Micro Aerial Vehicle	44
3.4.4 Optimization Techniques and Validation	45
4 Theory and Methodology	47
4.1 Material Choice	47
4.2 FreeCAD	48
4.3 VAP 3.5	48
4.4 XFOIL	48
4.5 Model Development	49
4.6 Wind Tunnel Testing	49
4.6.1 Wind Tunnel Setup	50
4.7 Stability Calculation	52

Table of contents

5 Results and Discussion	56
5.1 Wind Tunnel Results	56
5.1.1 Aerodynamic Coefficient of Lift	56
5.1.2 Aerodynamic Coefficient of Drag	57
5.1.3 Pitching Moment Coefficient	60
5.1.4 Yawing Moment Coefficient	61
5.1.5 Rolling Moment Coefficient	61
5.1.6 Static Margin	61
5.2 VAP Validation	61
5.2.1 Wing Validation	61
5.2.2 Model Validation	62
5.3 Discussion	64
References	65
Appendix A Work Health and Safety	79
A.1 Physical Health	80
A.2 Covid-19 precautions	82
A.3 Mental health	83

List of figures

1.1 MAV gross weight with wing span. Figure is adapted [1]. Image sources: [2] [3] [4] [5] [6] [7] [8] [9]	2
1.2 Examples of MAVs with category	2
2.1 Aircraft geometric parameters	7
2.2 Forward swept wings of Grumman X-29 (negative sweep angle) [10] . .	9
2.3 Wing dihedral and anhedral example. Image source: [11]	10
2.4 Wing twist and incidence angle	11
2.5 High and medium aspect ratio aircraft examples	12
2.6 Aircraft reference frames	14
2.7 Earth centered axes [12]	15
2.8 Pressure distribution over a wing	17
2.9 Aerodynamic forces acting on MAV	18
2.10 Lift curve with respect to angle of attack	19
2.11 Position of center of gravity (CG), neutral point (NP) and aerodynamic center (AC)	20

List of figures

2.12 General forces acting through the neutral point and center of gravity for a stable and unstable state	21
2.13 Relevant parameters when an aircraft undergoes a sideslip motion	23
2.14 Moments acting on an aircraft	24
2.15 Reynolds number parameters when describing the flow over a flat plate	25
2.16 Reynolds number parameters which induce the transition from laminar to turbulent flow	26
3.1 MAV speed with Reynolds number region in respect to flying bodies. Figure is adapted [13]. Image sources: [14] [15] [16] [17]	30
3.2 Flow characteristics across the propeller when the propeller is turned off (a) and when the propeller is turned on (b) [18]	31
3.3 Flow separation position change with Reynolds number [19]	33
3.4 Anatomy of laminar separation bubbles. Figure adapted from Mohamed [20]	34
3.5 a) Laminar flow to turbulence without surface roughness. b) Smaller transition region and turbulent boundary layer length with a rough surface. Figure is adapted [21].	35
3.6 Airfoil aerodynamic performance variation with increasing: (a) turbu- lence intensity (b) length scale [20]	36
3.7 Flow patterns shown by smoke. Laminar flow to turbulence without surface roughness (a). Laminar flow for with a rough surface (b). [21] . .	36

List of figures

3.8 Development of wingtip vortices over a wing section [22]	37
3.9 Tangential and Axial velocity effects [23]	39
3.10 Propeller slipstream effects on a finite wing [23]	39
3.11 Effect of propeller slipstream on the lift coefficient curve with angle of attack ($Re = 0.3 \times 10^5$) [24].	40
3.12 Propeller slipstream effect with span-wise location for airflow transition over the wing upper surface, $\alpha = 2.5^\circ$ [24].	41
3.13 Influence areas related to propeller-wing interaction based on the loading distributions [25]	42
3.14 Blade angle of attack variation due to propeller pitch angle [25]	43
3.15 GenMAV Model [26]	45
3.16 Unique constraints of MAVs [20]	46
4.3 Nano 25 load cell mount	50
4.1 Safety net to	51
4.2 Caption	52
4.4 Examples of MAVs with category	54
4.5 Callibrating pitch of model mount to ensure Aoa is accurate	55
5.1 Coefficient of lift variation with various conditions for the pusher, tractor and no propeller configurations	57

List of figures

5.2 Coefficient of drag variation at 11000RPM motor speed for the tractor, pusher and no propeller configurations	58
5.3 Coefficient of drag variation at 20ms airspeed for the tractor, pusher and no propeller configuration	59
5.11	62
5.13	63
5.12	63
A.1 Risk matrix.	80
A.2 Best posture at a desk.	82

List of tables

List of abbreviations

AC Aerodynamic Center.

AR Aspect Ratio.

CG Center of Gravity.

LABs Laminar separation bubbles.

NP Neutral Point.

Open VSP Open Vehicle Sketch Pad.

RPM Revolutions per minute.

Glossary

Generic micro-aerial vehicle .

Local-vertical local-horizontal .

Micro aerial vehicle .

Unmanned aerial vehicle .

Work health and Safety .

Chapter 1

Introduction

Unmanned aerial vehicles (UAVs) are used throughout various industries to conduct missions that are either dangerous, difficult or tedious for humans to perform. Recently UAVs have seen unprecedented growth for both commercial [27] and military [28] [29] use. The capability to fly within narrow spaces gives MAVs a significant advantage over general UAVs in specific use cases. MAVs, in particular, are more manoeuvrable in cluttered environments, such as, collapsed buildings, commercial centres, and search and rescue missions. Given current technology, MAVs could provide coordinates of trapped victims in areas where it would be dangerous to search manually [30]. Possible applications of MAVs include dangerous gas detection, environmental monitoring, border patrol, mapping, precision agriculture, homeland security, and drug interdiction [27] [30]. MAVs ability to be much quieter and concealed give it a major advantage over UAVs.

Today defence programs around the world utilize UAVs for reconnaissance, surveillance, damage assessments, and communication relay [28] [29] [30]. Miniature aerial vehicles (MAVs) have even more recently seen major research interest, particularly in the last decade [30]. The relative size of MAVs to other typical aircraft is shown in Figure 1.1. Smaller vehicles are intended to lower the total cost of systems currently used and increase the portability of MAVs [31]. The most limiting factors holding back MAVs from being more predominantly used, are propulsion, configuration, and flight control issues [31].

Introduction

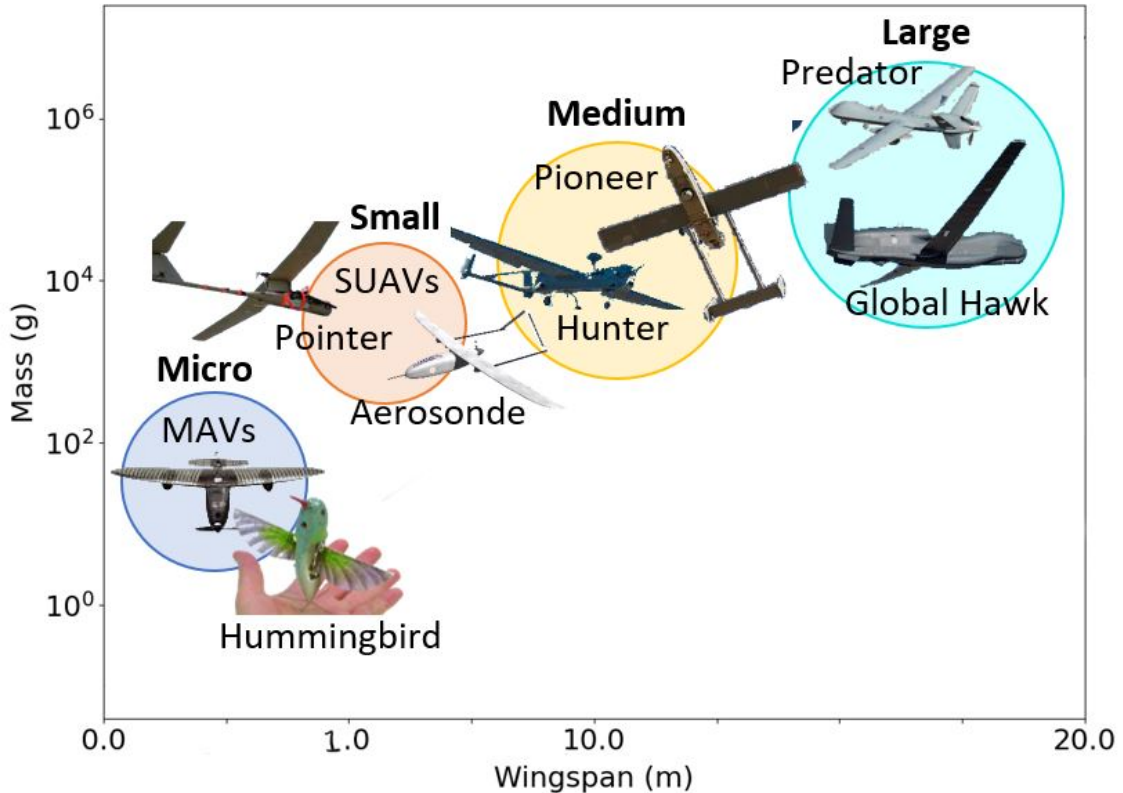


Fig. 1.1 MAV gross weight with wing span. Figure is adapted [1]. Image sources: [2] [3] [4] [5] [6] [7] [8] [9]

MAVs fall into three main categories. These are fixed wings [32], rotary wings [33] and flapping wings [34], which can also be used in combination.

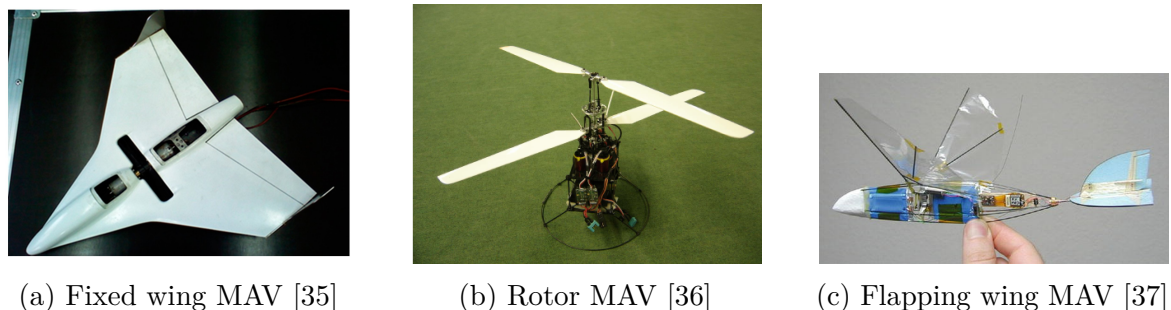


Fig. 1.2 Examples of MAVs with category

1.1 Problem Statement

MAVs are much more difficult to design and manufacture than typical aircraft [38]. This additional complexity is due to several factors:

- Low speed flight
- Small physical dimensions
- Structural strength
- Reduced stall speed due to smaller size
- Low inertia

With the increased complexity of MAV designs, there has also been an increased interest in the research and design of optimised MAV models [38]. Design software to optimise MAV designs is generally based on aerodynamic properties, weights, stability, and maneuverability [39] [40] [41]. The low-speed and non-linear flight dynamics are of particular importance for MAV development [42] [43]. The low speeds that MAVs fly at and the influence of an operating propeller on the rest of the MAV is currently unvalidated with physical wind tunnel testing. This thesis aims to fill in this gap.

1.1 Problem Statement

In the past, surveillance was conducted initially from hot air balloons. Later, aircraft such as helicopters would be used, costing companies large sums of money to survey from a bird's eye view [44]. Today drones and UAVs often conduct this work, within certain limits due to range and flight time [45] [44]. The next significant technology jump sees the optimisation and miniaturisation of these aircraft to produce MAVs. MAVs are set to increase the ability to conduct a variety of missions that predominately have military or surveillance objectives [44] [46] [47] [48].

Introduction

The MAV's main deferring attributes are; its smaller size, lower radar visibility and lower noise output. With MAV design becoming one of the fastest-growing areas of development in the aerospace industry, there is an increasing need to have accurate experimental data to validate, simulate and model the numerous MAV configurations being investigated. One of the core but currently missing pieces to this puzzle is the influence and effect of propellers on the aerodynamics and stability of MAVs. Can we further deepen our understanding of MAVs by analysing these effects?

1.2 Objectives

The objectives of this thesis are as follows:

1. To carry out a review of current published literature and determine areas with insufficient or no research available for further development and research.
2. To design and produce a 3D model of a MAV with an interchangeable empennage.
3. To conduct wind tunnel testing of the MAV model with and without propeller effects.
4. To analyse data of wind tunnel results and detail the effect that propellers have on the MAV model.

1.3 Outline

An outline of the proposed final submission is listed below. However, it is subject to change.

- Chapter 2: Background

1.3 Outline

- Chapter 3: Literature Review
- Chapter 4: Proposed Setup of Analysis
- Chapter 5: Implementation
- Chapter 6: Results
- Chapter 7: Discussion

Chapter 2

Background

This chapter outlines the core theory and topics relevant for optimising MAVs and relevant literature regarding the effect of propeller interactions on MAVs. Crucial coefficients, concepts and terminology are explained here. This section will cover general aircraft geometry, aerodynamic forces, reference frames, longitudinal stability, lateral stability and Reynolds number.

2.1 Aircraft Geometry

Several aircraft geometric parameters will be referred to throughout this thesis. Key parameters discussed are the wingspan, chord length, aspect ratio, sweep, dihedral and twist. Figure 2.1 shows some of these.

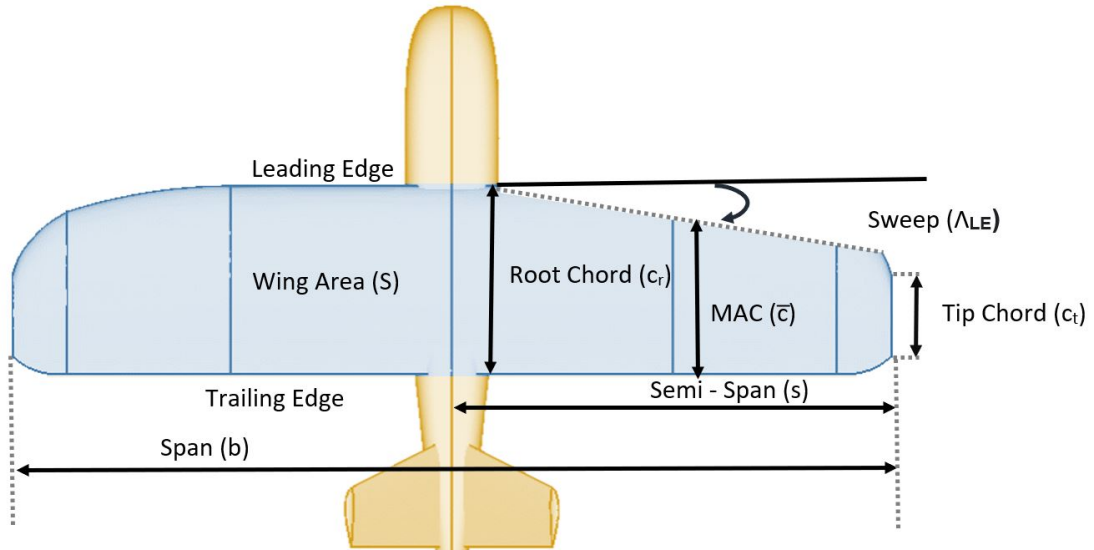


Fig. 2.1 Aircraft geometric parameters

2.2 Span

The wingspan (b) is the distance from one wing tip to the other. The semi-span (s) is the distance from the fuselage reference line to the wing tip. These parameters are also shown in Figure 2.1.

2.3 Chord

The chord is the distance between the leading and trailing edge of the wings shown in Figure 2.1. The chord is often defined in terms of three main parameters, these are:

- **Root Chord (denoted c_r):** This is the chord length where the wing meets the fuselage and is generally the position where the chord length is the longest.

Background

- **Tip Chord (denoted c_t):** The tip chord is the chord length at the tips of the wings
- **Mean Aerodynamic Chord (MAC):** The mean aerodynamic chord is used to represent the wing in only two dimensions. The MAC is the chord length at which the resultant aerodynamic force acts. The MAC is defined by Equation 2.1 and is taken from wing tip to wing tip. In the case of a straight tapered wing with a taper ratio, the MAC equation can be simplified to Equation 2.2.

$$\bar{c} = \frac{\int_0^b c(y)^2 dy}{\int_0^b dy} \quad (2.1)$$

$$\bar{c} = \frac{2c_r(1 + \lambda + \lambda^2)}{3(1 + \lambda)} \quad (2.2)$$

The taper ratio defines the ratio between the root and tip chord lengths. The taper ratio is given by Equation 2.3.

$$\lambda = \frac{c_t}{c_r} \quad (2.3)$$

The taper ratio is significant as it influences the lift distribution over the wing. By reducing the wing area towards the wing tips, the moment produced by the wings is reduced.

2.4 Sweep

The sweep is the angle (Λ_{LE}) between the y_b axis and the leading edge. When wings are swept back, the flow is directed outwards along the length of the wing. This

2.4 Sweep

also changes the angle of attack towards the wings' tips. A negative sweep angle (generally only seen on experimental aircraft such as the Grumman X-29 shown in Figure 2.2) directs the flow inboard towards the fuselage. Sweep is also used to assist with static longitudinal stability. A positive sweep angle will move the aircraft's centre of gravity backwards and vice versa. The sweep angle (Λ_{LE}) can be used to fine-tune the pitch stability. Sweep is also used to delay shock wave formation on wings. In this phenomenon, at high Mach numbers (> 0.8), a sharp discontinuity of pressure is seen in a narrow region travelling through a medium.



Fig. 2.2 Forward swept wings of Grumman X-29 (negative sweep angle) [10]

Background

2.5 Dihedral

The dihedral angle (γ) is the angle between the wing and the y_b axis, which is represented by the horizontal dotted line in Figure 2.3. A dihedral angle is when the wing tip is at a higher point than the root of the wing. This is the opposite for the case of an anhedral angle, also shown in Figure 2.3. Having a dihedral angle increases the lateral stability - particularly when banking, as the lower wing will fly at a higher angle of attack than the higher wing.

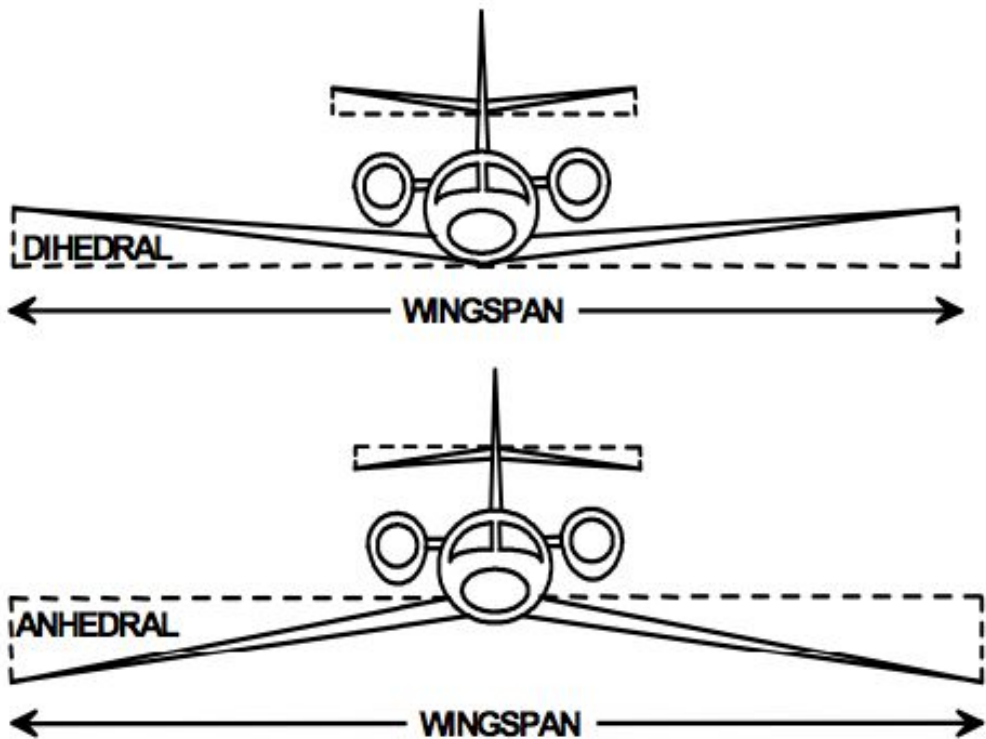


Fig. 2.3 Wing dihedral and anhedral example. Image source: [11]

2.6 Twist and Incidence

The wing twist angle (θ_t) is the angle between the tip chord reference line and the root chord. By convention, a positive wing twist angle is defined as a downward twist on the wing. Figure 2.4 shows an example of this. Another significant parameter is the wing incidence angle (θ_i) which is the angle between the fuselage reference line and the root chord line. In this case, a positive incidence angle is defined as an upward twisted root chord.

The wing twist is often used to redistribute the lift along the wing's surface. The wing tip is the last wing surface that will experience stall; particularly when in a steep climb or roll manoeuvre. By twisting the wingtip downwards with respect to the rest of the wing, the effective angle of attack will be lower at the wingtip than at the root. This means that the root will stall before the wingtip. This is desirable as control surfaces such as ailerons lose their effectiveness when the wingtips stall first.

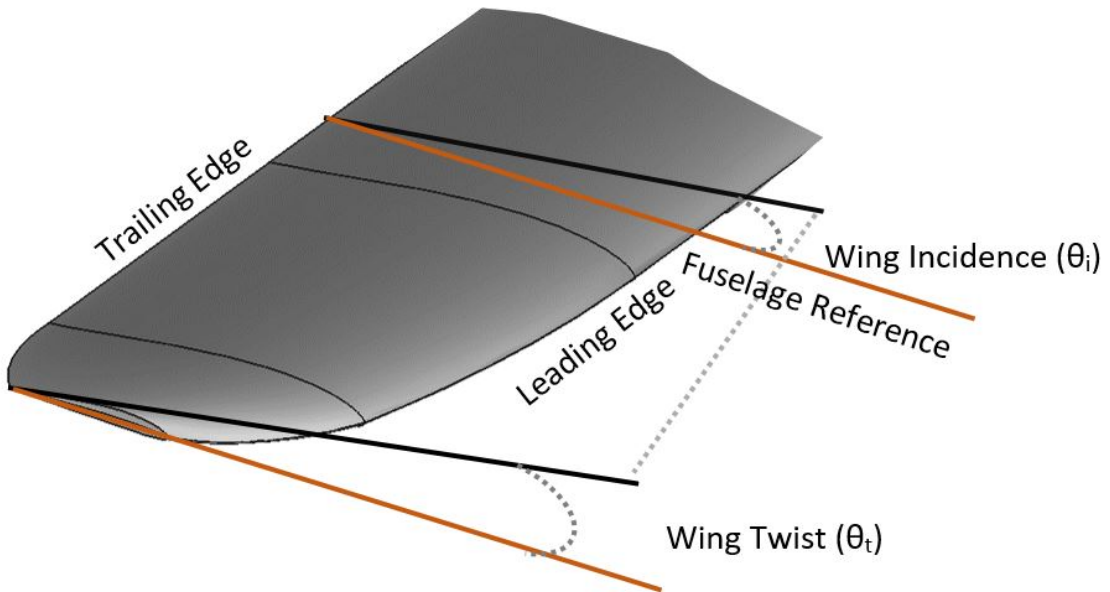


Fig. 2.4 Wing twist and incidence angle

Background

2.7 Aspect Ratio

The aspect ratio (AR) is significant when considering an aircraft's aerodynamic efficiency. First, the wing area (S) must be introduced. The AR can be calculated through Equation 2.4.

$$AR = \frac{b^2}{S} \quad (2.4)$$

Where b is the wing span and S is the total platform area of the wing, also shown in Figure 2.1, as the area coloured blue.

Higher aspect wings produce less lift-induced drag - however, they often require more structural support and are typically heavier than lower AR aircraft. High aspect wings are long and thin, whilst low aspect wings are short and wide. Figure 2.5 shows two aircraft with high and medium ARs. The Schleicher aircraft shown has a much higher AR. This also means it has high aerodynamic efficiency.

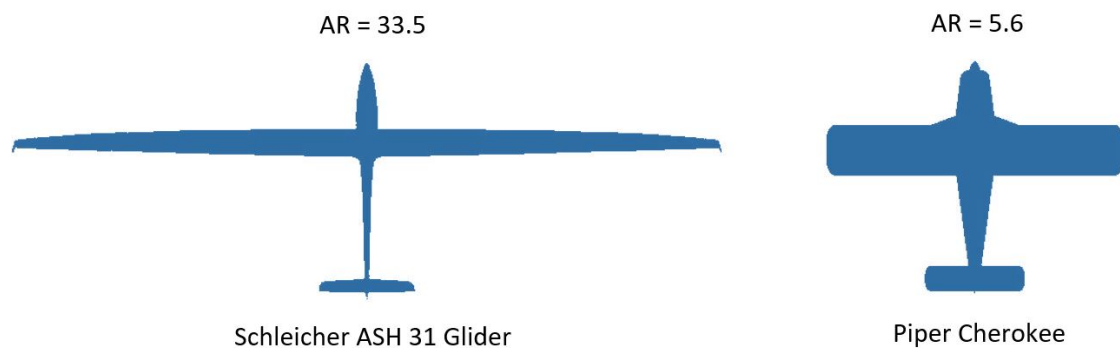


Fig. 2.5 High and medium aspect ratio aircraft examples

2.8 Reference Frames

The primary reference frames used to describe the position of an aircraft are:

- Earth Centered Axes
- Local-vertical local-horizontal (LVLH) Axes
- Body Axes
- Stability Axes
- Air Axes

Figure 2.6 provides a visualisation to assist with the following explanations.

Background

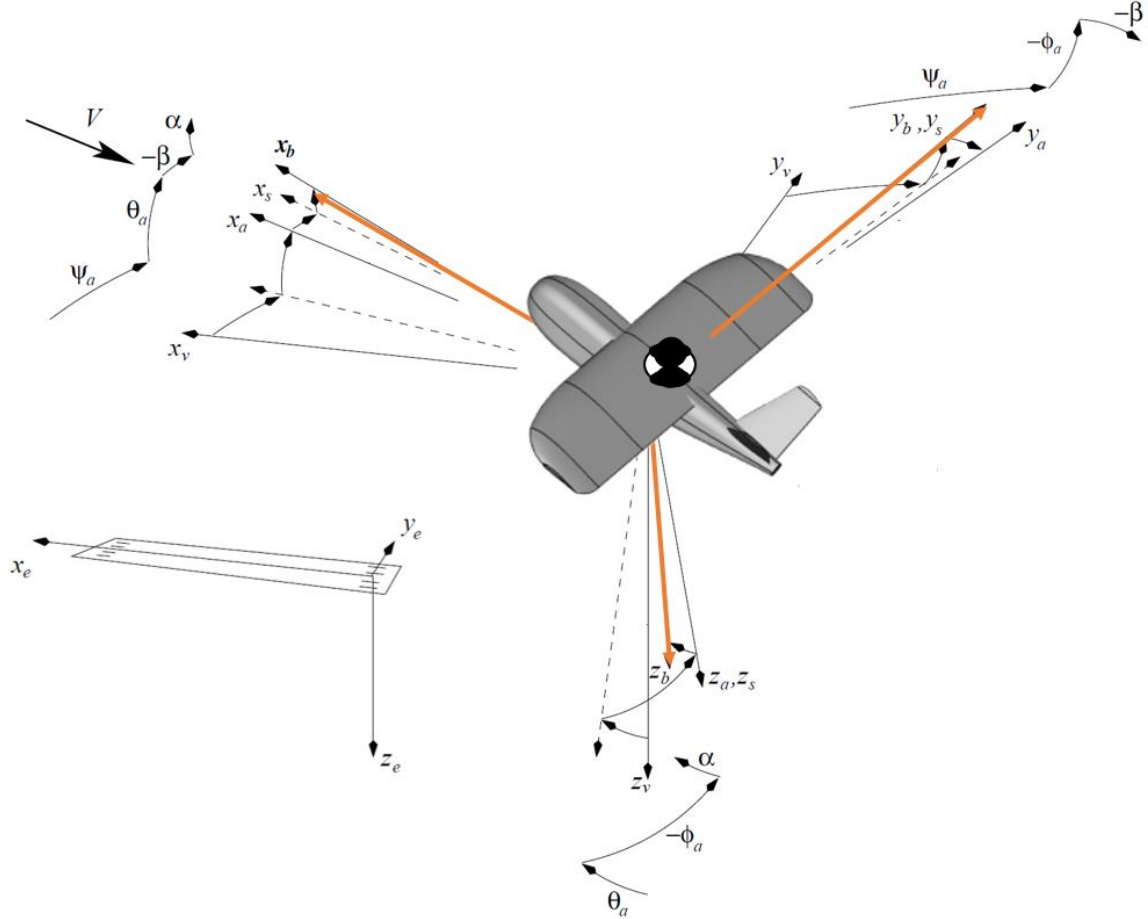


Fig. 2.6 Aircraft reference frames

2.9 Earth Centered Axes: denoted as (x_e, y_e, z_e)

The Earth centered axes is a global reference frame with the centre of the Earth's origin. From the Earth's centre, three orthogonal axes remain fixed to the Earth. This axis is primarily used when describing the position of aircraft. Further visualisation of this reference frame is shown in Figure 2.7. As Earth has an ellipsoid shape (rather than a sphere), the position is described in terms of the latitude (ϕ), longitude (λ), and altitude (h).

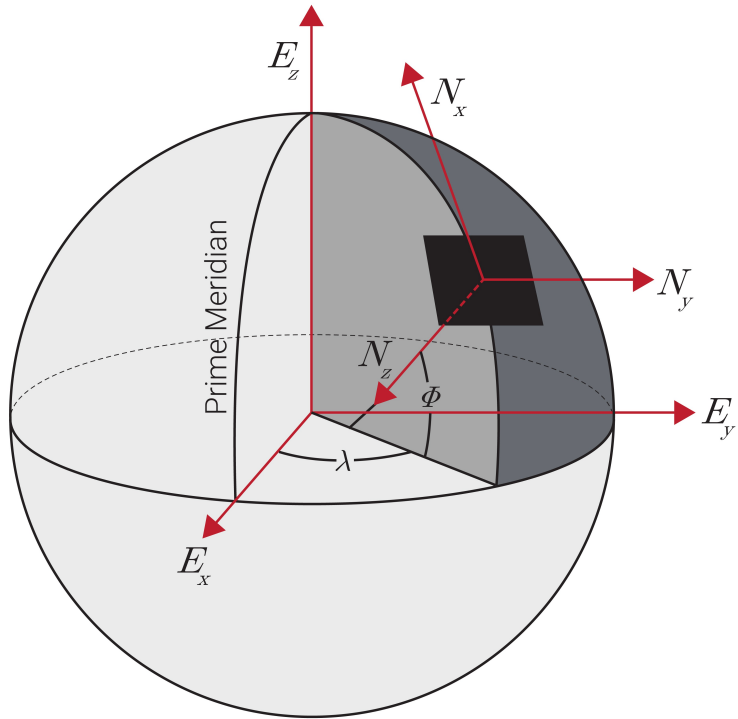


Fig. 2.7 Earth centered axes [12]

2.10 LVLH Axes: denoted as (x_v, y_v, z_v)

This axis frame translates with the aircraft and is aligned with the Earth axes previously described. It is shown in Figure 2.6.

2.11 Body Axes: denoted as (x_b, y_b, z_b)

This axis is positioned at the aircraft's centre of gravity. Figure 2.6 shows this position in the aircraft's centre. The body axes translate with the aircraft and are highlighted in orange in Figure 2.6.

Background

2.12 Stability Axes: denoted as (x_s, y_s, z_s)

The stability axis has its origin at the centre of gravity, shown in Figure 2.6. It translates with the aircraft's movement. x_s aligns with the air path and is described as an offset from x_b by an angle of α (further described in 2.14). y_s is aligned with the body axes y_b and z_s acts perpendicular to both x_s and y_s .

2.13 Air Path Axes: denoted as (x_a, y_a, z_a)

The air path axis has its origin at the centre of gravity. x_a is aligned with the relative air path and is offset from x_b by the angle of attack (α). y_a is also aligned with the relative air path and is offset from the y_b by the sideslip angle (β). z_a is perpendicular to both x_a and y_a .

2.14 Key Parameters

Some key parameters are used to define the motion of the aircraft. These are explained below:

- **Aerodynamic Angles (α, β) :** These angles are used to describe the offset of the aircraft's body axes to the relative air path. α is also known as the angle of attack and describes the angle between the x_a and x_b positions. β is also known as the side slip angle and describes the angle between the y_a and y_b positions. These angles are also shown in Figure 2.6.
- **Euler Angles $(\theta_a, \phi_a, \psi_a)$:** The Euler angles are used to describe the orientation of rigid bodies with respect to a fixed coordinate system. In the case of aircraft,

2.15 Aerodynamic Forces and Coefficients

this describes the pitch (θ_a), yaw (ψ_a) and roll (ϕ_a). These angles are relative to the LVLH reference frame. These can be seen in Figure 2.6.

2.15 Aerodynamic Forces and Coefficients

Airfoils which are designed to produce lift, achieve this by creating a pressure difference between the upper and lower surface when moving through a fluid. This lift force acts perpendicular to the chord line and is shown in Figure 2.8.

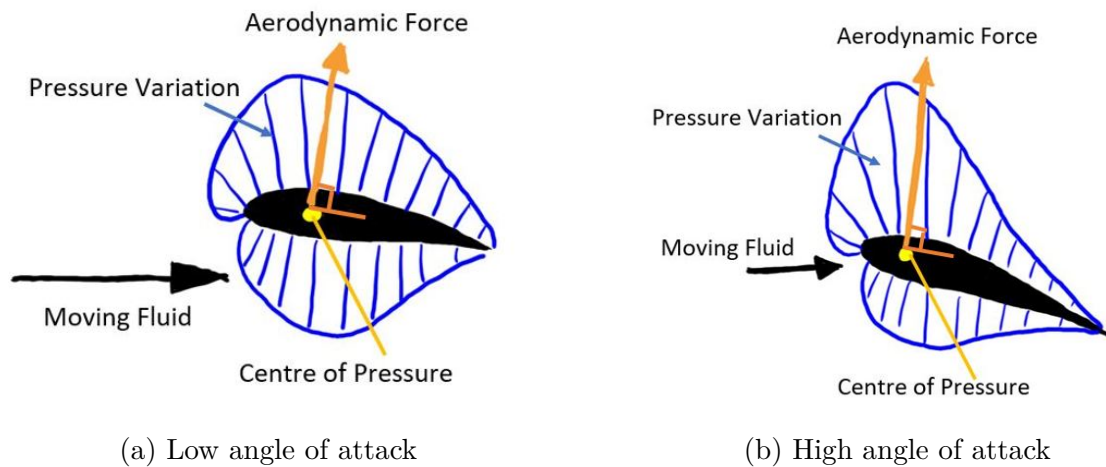


Fig. 2.8 Pressure distribution over a wing

In order to simplify calculations regarding this force distribution, the aerodynamic centre is used. The wing's aerodynamic centre is the wing's position where when the net force is applied, the total moment created with respect to the angle of attack remains constant. Through these simplifications, the total force acts through a single point - the aerodynamic centre. The main forces which act on the wing are lift and drag. Lift (L) is the force acting normally on the air path axes (z_a). Drag (D) is the force that acts both in the x_a , air path axis and long the aircraft surface due to air

Background

friction. The main components for the aerodynamic forces and coefficients are the wing, tail and fuselage. The main forces are also shown in Figure 2.9.

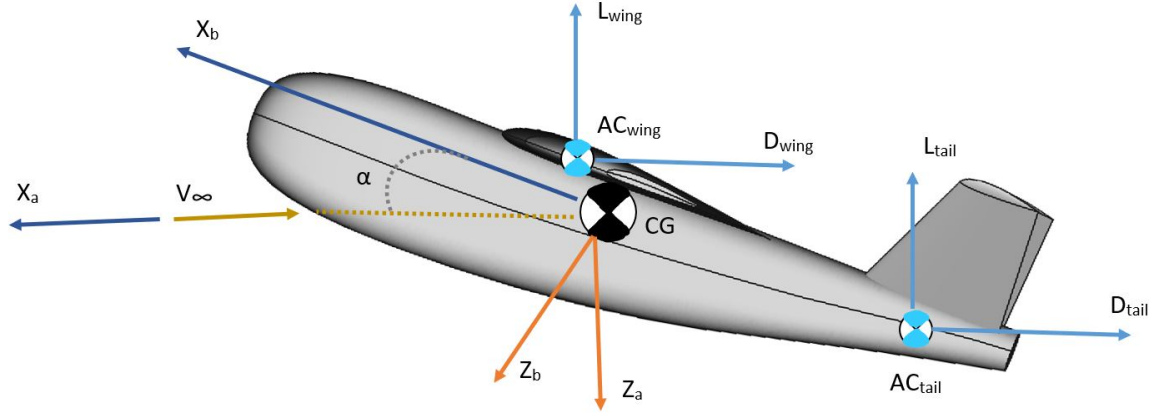


Fig. 2.9 Aerodynamic forces acting on MAV

Two significant aerodynamic coefficients are used as the lift and drag forces coefficients shown in Equations 2.5 and 2.6. These coefficients are the lift and drag forces when normalised by the dynamic pressure (q) and the wing area (S).

$$C_L = \frac{L}{qS} = \frac{L}{\frac{1}{2}\rho V_\infty^2 S} \quad (2.5)$$

$$C_D = \frac{D}{qS} = \frac{D}{\frac{1}{2}\rho V_\infty^2 S} \quad (2.6)$$

The lift coefficient can also be described in terms of the angle of attack, the lift coefficient at an angle of attack of 0 (C_{L_0}) and the slope of the lift curve with respect to the angle of attack (C_{L_α}).

$$C_L \approx C_{L_0} + C_{L_\alpha} \alpha \quad (2.7)$$

2.16 Static Longitudinal Stability

Figure 2.10 shows a visualisation of these parameters.

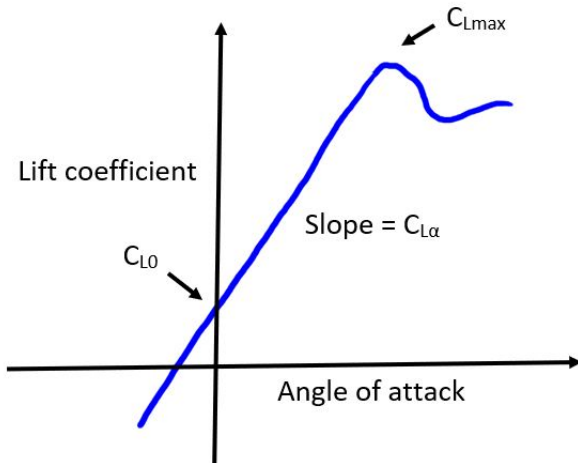


Fig. 2.10 Lift curve with respect to angle of attack

Equation 2.7 is accurate at small angles of attack where the lift curve slope is linear as shown in Figure 2.10. The lift curve slope at higher angles of attack becomes non-linear due to flow separation, and hence Equation 2.7 is an inaccurate approximation. Drag can be estimated through Equation 2.8, where C_{D_0} is the drag due to skin friction and e is the Oswald efficiency factor. The Oswald efficiency factor measures the lift distribution efficiency across a wing.

$$C_D \approx C_{D_0} + \frac{C_L^2}{\pi AR e} \quad (2.8)$$

2.16 Static Longitudinal Stability

Static longitudinal stability is determined from the pitching moment M . The pitching moment is defined as shown in Equation 2.2.

Background

$$C_M = \frac{M}{\frac{1}{2}\rho V_\infty^2 S c} \quad (2.9)$$

The derivative of the pitching moment with respect to the angle of attack must be negative with a positive angle of attack to be stable. This is also given in Equation 2.10.

$$C_{M\alpha} = \frac{\delta C_M}{\delta \alpha} < 0 \quad (2.10)$$

The aerodynamic centre of the aircraft is also referred to as the neutral point. The total aerodynamic force acts through the neutral point and is the position where no change in pitching moment is seen with a variation in the angle of attack ($C_{M\alpha} = 0$ when $x_{cg} = N_0$). Figure 2.11 shows the parameters on the aircraft. When the position of the centre of gravity is the same as the neutral point, the aircraft is neutrally stable.

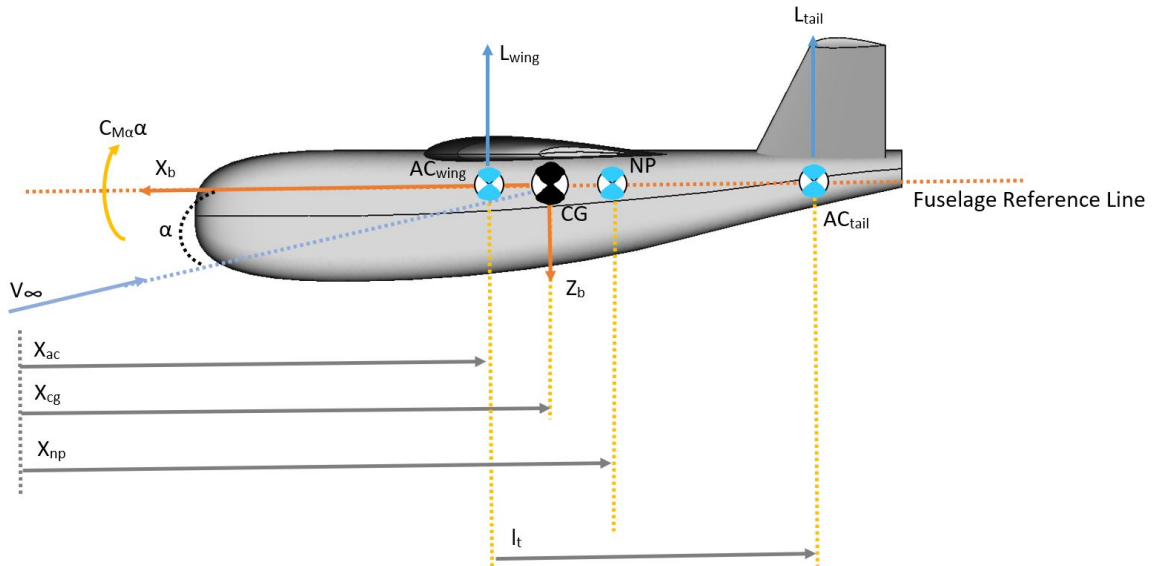


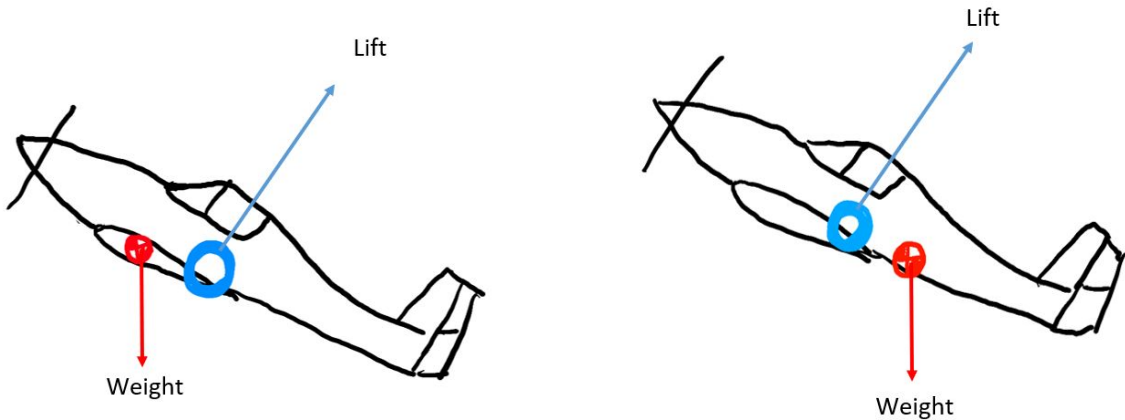
Fig. 2.11 Position of center of gravity (CG), neutral point (NP) and aerodynamic center (AC)

2.16 Static Longitudinal Stability

Another important concept for stability is the static margin. The static margin is defined as the distance between the neutral point and the centre of gravity indicated in Figure 2.11. The static margin is expressed as a percentage of the mean aerodynamic chord length and is given in Equation 2.11. A large static margin indicates that an aircraft is stable.

$$C_{M\alpha} = C_{L\alpha} \left(\frac{x_{cg}}{c} - N_0 \right) \quad (2.11)$$

If the centre of gravity is positioned too far forward, the pitching stiffness coefficient becomes negative with a large magnitude. Aircraft in this state require large control surface deflections to be manoeuvrable. Aircraft are designed with this stability in mind, and the pitch stiffness is placed within reasonable controllability and stability limitations. Figure 2.12 shows the stability difference when moving the center of gravity and neutral point locations.



(a) When the center of gravity is ahead of the neutral point then the weight tends to correct this displacement (stable).

(b) When center of gravity is behind the neutral point the weight worsens the displacement (unstable).

Fig. 2.12 General forces acting through the neutral point and center of gravity for a stable and unstable state

2.17 Static Lateral Stability

Static lateral stability is determined by the roll moment L and yaw moment N . Similarly to how the lift and drag coefficients were normalised, the roll and yaw moments can be normalised to form their coefficient forms. These Equations are given in 2.12 and 2.13.

$$C_L = \frac{L}{\frac{1}{2}\rho V_\infty^2 S b} \quad (2.12)$$

$$C_N = \frac{N}{\frac{1}{2}\rho V_\infty^2 S b} \quad (2.13)$$

The lateral stability of an aircraft is based on the change in C_N and C_L with respect to disturbances in the sideslip angle. A further parameter can be determined from the yaw moment by taking the derivative with respect to the sideslip angle. This is given in Equation 2.14. This is also known as yaw stiffness.

$$C_{n_\beta} = \frac{\delta C_N}{\delta \beta} > 0 \quad (2.14)$$

A positive sideslip angle change for directional stability must produce a positive yaw moment change. A positive yaw moment shifts the aircraft to re-align the body and wind axes, reducing the sideslip angle. This is described in Equation 2.14.

Similarly, the derivative of the roll moment with respect to the sideslip angle can be used to determine the dihedral effect shown in Equation 2.15.

$$C_{l_\beta} = \frac{\delta C_l}{\delta \beta} < 0 \quad (2.15)$$

2.17 Static Lateral Stability

A positive sideslip angle change will produce a negative rolling moment to be laterally stable. This causes an aircraft to roll away from the relative wind flow. Hence a yawing movement to align with the air path is produced. This condition is given in Equation 2.15.

However, it is possible to have an aircraft that meets these criteria but is still hard to control. If the yaw or roll is too stiff (i.e. $C_{N\beta}$ is positive with a large magnitude and $C_{L\beta}$ is negative with a large magnitude), then the aircraft can still become impossible to manoeuvre. Hence the limitations of $C_{N\beta}$ and $C_{L\beta}$ are primarily limited by the actual controllability of the aircraft.

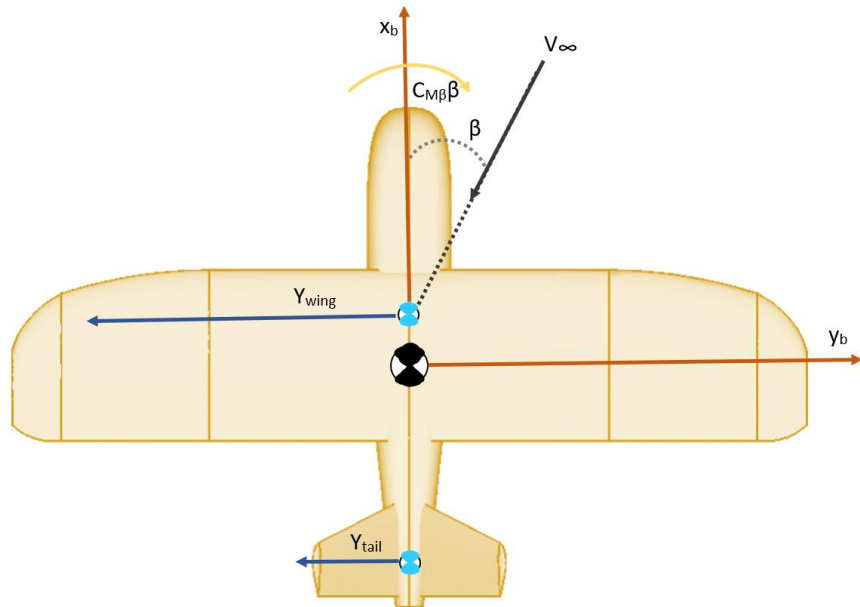


Fig. 2.13 Relevant parameters when an aircraft undergoes a sideslip motion

Background

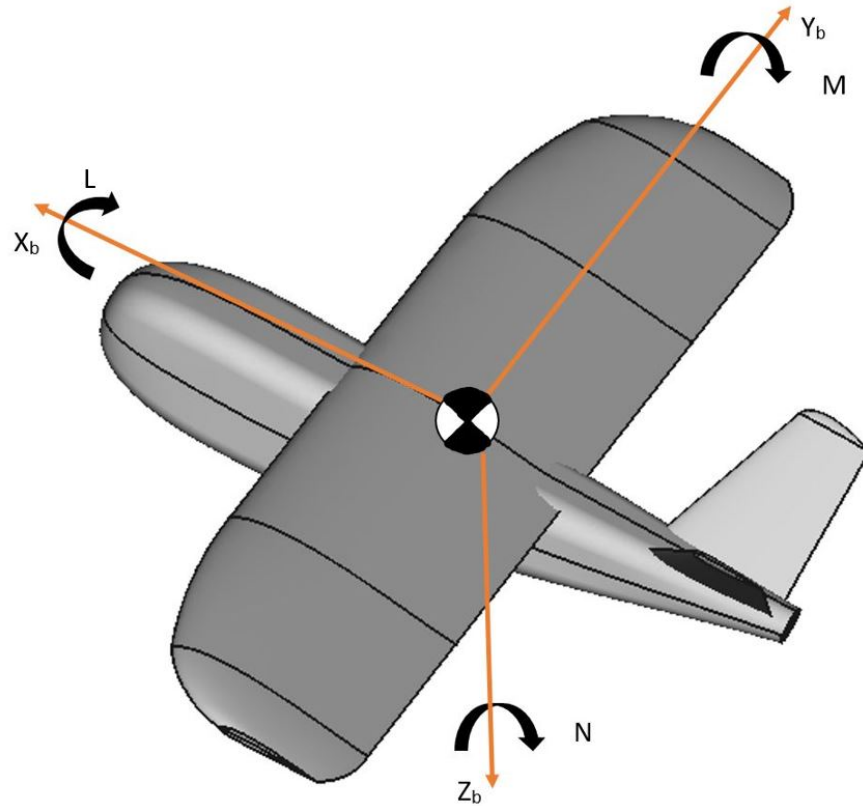


Fig. 2.14 Moments acting on an aircraft

2.18 Reynolds Number

Reynolds number is a dimensionless number used to represent the ratio of inertial forces to viscous forces. It is expressed in Equation 2.16 where:

- ν represents the kinematic viscosity of the fluid.
- ρ represents the density of the fluid (air in this case).
- u is the flow speed.
- L is a characteristic length. In the case of aircraft, this is typically the width of the frontal area being investigated.

2.18 Reynolds Number

- μ is the dynamic viscosity of the fluid.

$$Re = \frac{\rho u L}{\mu} = \frac{u L}{\nu} \quad (2.16)$$

Figure 2.15 shows a visualisation of these parameters.

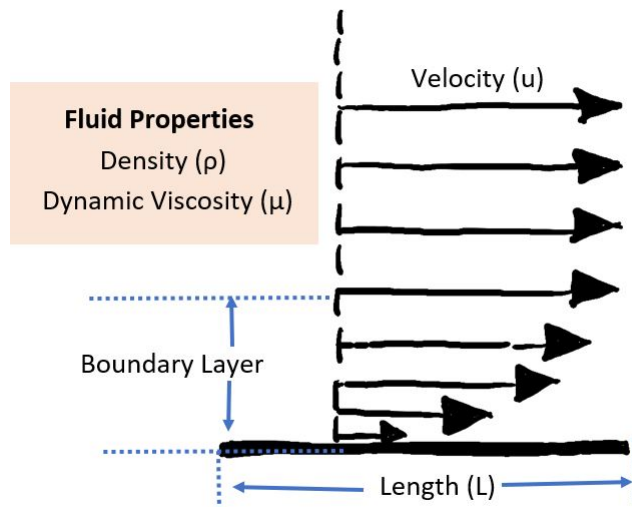


Fig. 2.15 Reynolds number parameters when describing the flow over a flat plate

The Reynolds number is a parameter for describing the flow of the fluid being investigated. It is often used when describing flow transitions from laminar to turbulent flow and other general fluid transitions. An example is shown in Figure 2.16.

Background

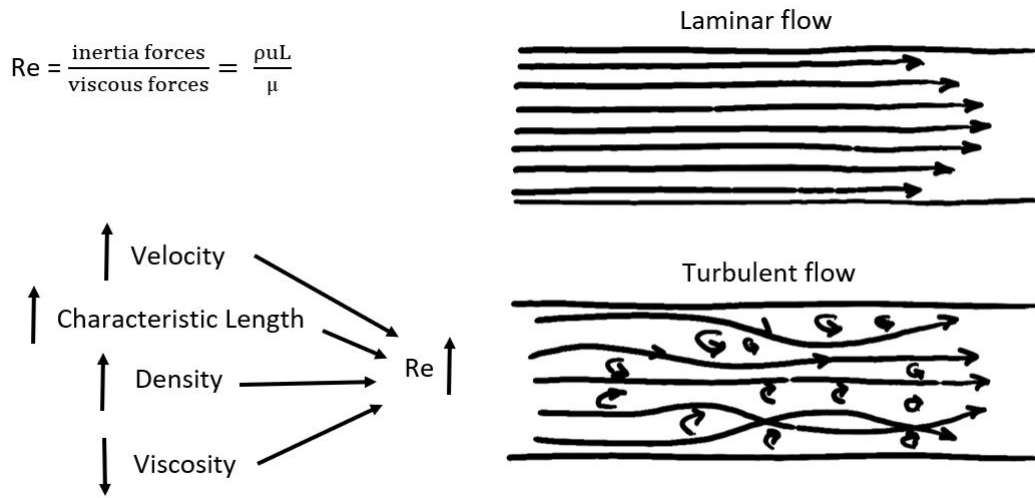


Fig. 2.16 Reynolds number parameters which induce the transition from laminar to turbulent flow

High Reynolds values ($> 10^6$) indicate that the viscous forces only account for a small amount of the flow and hence the flow is essentially inviscid. For low Reynolds number values ($< 10^5$), the viscous forces account for a significant portion of the flow and must be considered.

Chapter 3

Literature Review

This chapter contains a review of the current literature published on MAV development and the extent to which propeller effects have been researched. It explores the effects that propellers have on MAVs, current research on non-linear lift distributions, separation bubbles and propeller interactions and effects.

3.1 Proliferation of MAV's in the Aerospace Landscape

Initially introduced during World War I, UAVs were heavily criticized due to inaccuracies and unreliability when performing missions. Few saw the potential and impact they could have in changing the landscape of a battlefield [49]. UAVs have existed for centuries, although the modern era of UAVs commonly refers to the last four decades [50].

It was not until Operation Desert Storm (1991) and the Balkan Peninsula conflict that the development and interest in UAVs took off [49] [51]. The United States, the most predominant and invested country researching in UAV technologies (accounting for up to 77% of worldwide spending on UAVs [49] over the last decade). The U.S. at the time saw a total income of \$2.27 billion dollars [49] (a 9.5% increase from the previous year of 1996). This marked a turning point in the the development of more complex

Literature Review

UAVs [52] as the U.S. Department of Defense funded UAV research for the first time in 1996 [53]. The recent shift to the miniaturisation of components, systems and aerial vehicles has already influenced the military sector [44] [46], with several developments underway to reduce the visibility of reconnaissance aircraft and reduce the likelihood of aircraft being detected during missions [47] [48]. The most famous military MAV arguably being the Honeywell RQ-16 T-Hawk [54] which was mainly used by the U.S. forces in Iraq in order to search for roadside bombs [55]. The success of which (largely due to its hovering feature) led the U.S. Navy to order a further 372 MAVs [56].

What started as a small initial interest in smaller and smarter drones has resulted in exponential growth in the sector [45] [57]. Technology improvements have led to the exponential growth in the capabilities of MAV seen today [58] [59]. Where an initial drone supported only low camera resolution with meagre flight times, today incorporates several systems such as gyro stabilisation, GPS capability with way-point guidance, beyond the line of vision control, speeds of 70 km/h with a 30 minute flight time, and a 20-megapixel camera (DJI Phantom 4) [60].

3.2 Limitations of MAV Design Techniques

While MAV technology is more accessible and viable to the mass market than it has ever been before [59], there is no fully developed and validated way to optimize a MAV for a specified mission [61] [62]. Today, procedures involve developing a CAD model of the MAV or using software based on aerodynamics. This model is either then run through aerodynamic optimization software and/or tested in a wind tunnel to determine the main characteristics of the MAV [63]. The largest drawback of which is the lack of propeller effects accounted for, which are known to have a large effect on aerodynamics and stability [64] [65]. MAV model tests have been conducted with a fixed position propeller [66] [67]. Models are, however, typically tested without

3.3 Low Reynolds Number Effects

a free-flowing propeller, although these have been included in several aerodynamic software programs and specific tests [42].

However, a lack of validation from wind tunnel testing means that a full understanding of the effects a propeller has on MAVs has not been achieved. MAVs are small relative to the size of the propellers used. Hence, the propeller will significantly affect the stability, noise, overall endurance, performance and power consumption of a given MAV [68] [69].

3.3 Low Reynolds Number Effects

Due to the small size and Reynolds numbers at which MAVs operate (typically around $Re=10^5$ [70] [19]), insects and other small animals are often studied to understand the flight dynamics which occur for small flying bodies [71]. The Reynolds region in which MAVs typically fly is shown in Figure 3.1.

Literature Review

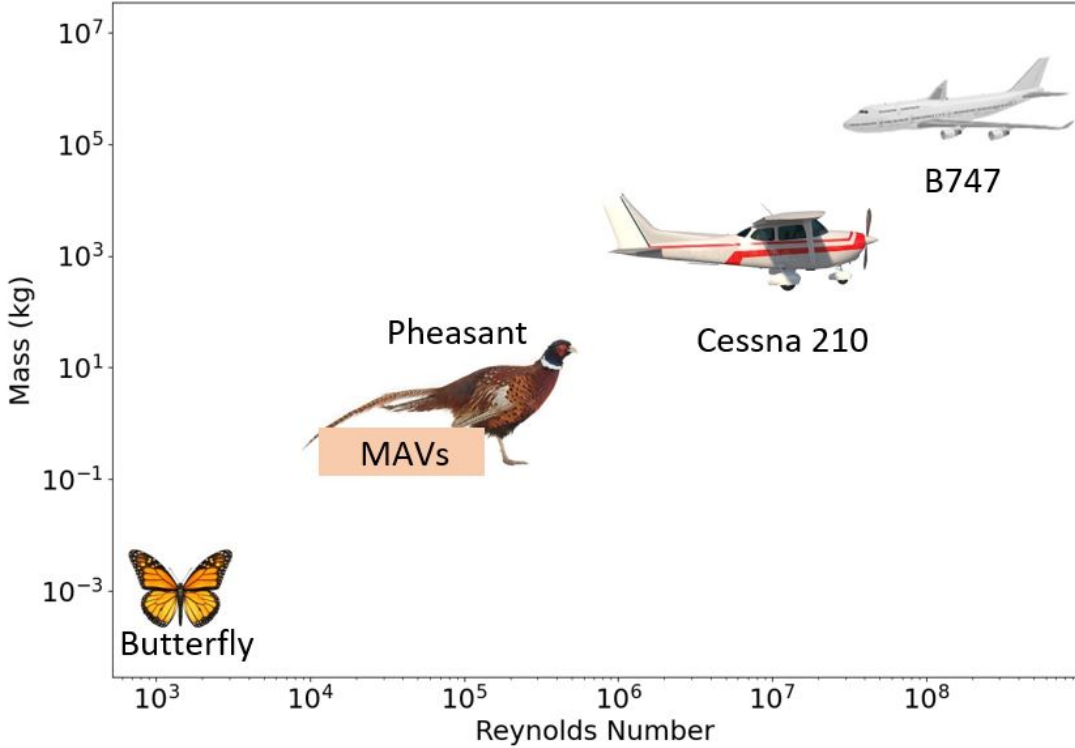


Fig. 3.1 MAV speed with Reynolds number region in respect to flying bodies. Figure is adapted [13]. Image sources: [14] [15] [16] [17]

Null used wind tunnel tests to show that propellers on wings during low Reynolds flight increased the performance of the wing at high angles of attack [72]. Ananda also visualised this effect as shown in Figure 3.2, however this is without the propeller being mounted on the wing directly.

3.3 Low Reynolds Number Effects

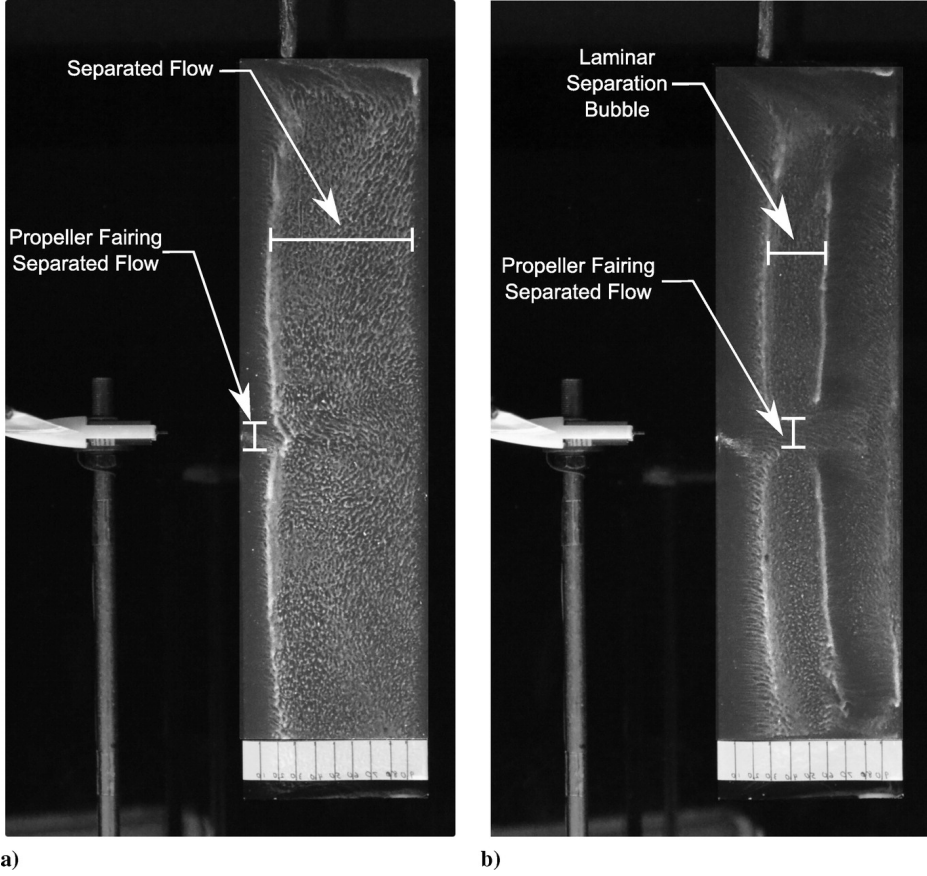


Fig. 3.2 Flow characteristics across the propeller when the propeller is turned off (a) and when the propeller is turned on (b) [18]

Low Reynolds number compressible aerodynamics affect wide different varieties of aircraft. Aircraft used to survey martian terrain and MAVs are mainly influenced due to the change in atmosphere and small geometry respectively [73]. Low Reynolds number effects are critical for propeller based MAV systems. As the root and tip of a propeller can differ significantly in Mach number [73]. As MAVs have small ARs due to their smaller size and non-conventional structures, low AR wings at low Reynolds numbers have recently, in particular, been studied [74] [75]. Cosyn showed that the flow over these is characterised by complex 3D phenomena such as wing-tip vortices, laminar to turbulent transitions, and flow separation, and re-attachment [76].

Literature Review

Airfoils in particular have been investigated due the importance of their use in aircraft. At low Reynolds numbers ($10,000 < \text{Re} < 50,000$) the flow remains laminar when the airfoil is aligned with the incoming flow. Pressure gradients created due to a larger angle of attack or high camber (airfoil thickness) create turbulent flow following separation. This is also shown in Figure 3.3. Early research by Mueller showed that the maximum lift coefficient is typically 0.5 for airfoils before stalling at low Reynolds numbers [77].

At Reynolds numbers from 50,000 to 100,000 the separation bubble and turbulent layer thickness increase in size [19]. The separated shear layer will eventually gain enough momentum from the free-stream in order to reattached to the airfoil as shown in Figure 3.3. The separation bubble is also known as a laminar separation bubble (LSB). Mueller found that airfoil choice in this region was critical to the aerodynamic performance. Airfoils with large camber (thickness) produce large pressure gradients causing separating which leds to the formation of LSBs on the upper surface of the wing [77]. As Reynolds numbers increases the separation and attachment move towards the leading edge [19]. The turbulent layer thickess reduces and the airfoil performance improves. The turbulent layer thickness varies between airfoils and LSBs can still form up until around a Reynolds number of 200,000. This is notable as most MAVs operate around the 50,000 to 200,000 Reynolds number range [78]. At Reynolds numbers greater than 500,000 the separation point generally lies on the leading edge. The performance of airfoils increases due to the reduced turbulent layer. Separation however can occur at high angles of attack. Turbulent boundary layer initially separates from the tailing edge but this separation will move towards the leading edge as the angle of attack increases. This can lead to stall of the entire airfoil [19].

3.3 Low Reynolds Number Effects

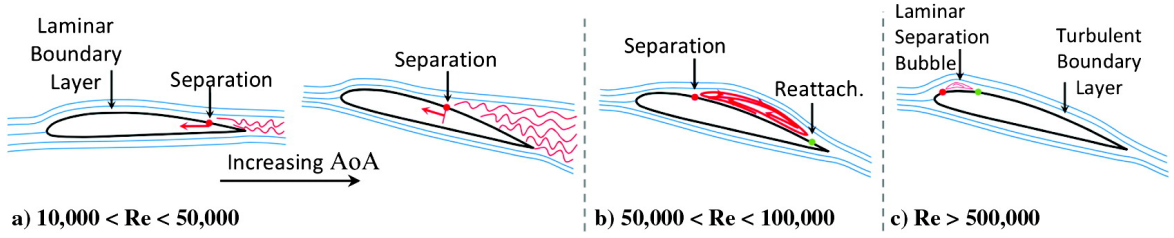


Fig. 3.3 Flow separation position change with Reynolds number [19]

3.3.1 Laminar Separation Bubbles and Vortices

Flow separation and re-attachment create separation bubbles over wings and account for the most drag over the surface of wings at these low Reynolds numbers [79]. LSBs typically occur at Reynolds number below 200,000. Perot showed how in the presence of adverse pressure gradients, airflow separates from the wing, this was further validated by Mohamed [20] [80]. The flow can either reattach or remain separated, which in turn produces turbulent flow [81]. Mohamed investigated these LSBs and showed that they can deteriorate a MAVs stability as the drag induced by these bubbles leads to a low-pressure region over the bubbles, causing severe perturbations of motion [20]. Marxen further provided an explanation as to why these bubbles are typically stable, as no transfer of energy occurs between the flow circulating inside the bubble and the laminar flow, which passes over the top [82]. Detailed anatomy of how LSBs affect flow over a typical airfoil shape is shown in Figure 3.4.

Literature Review

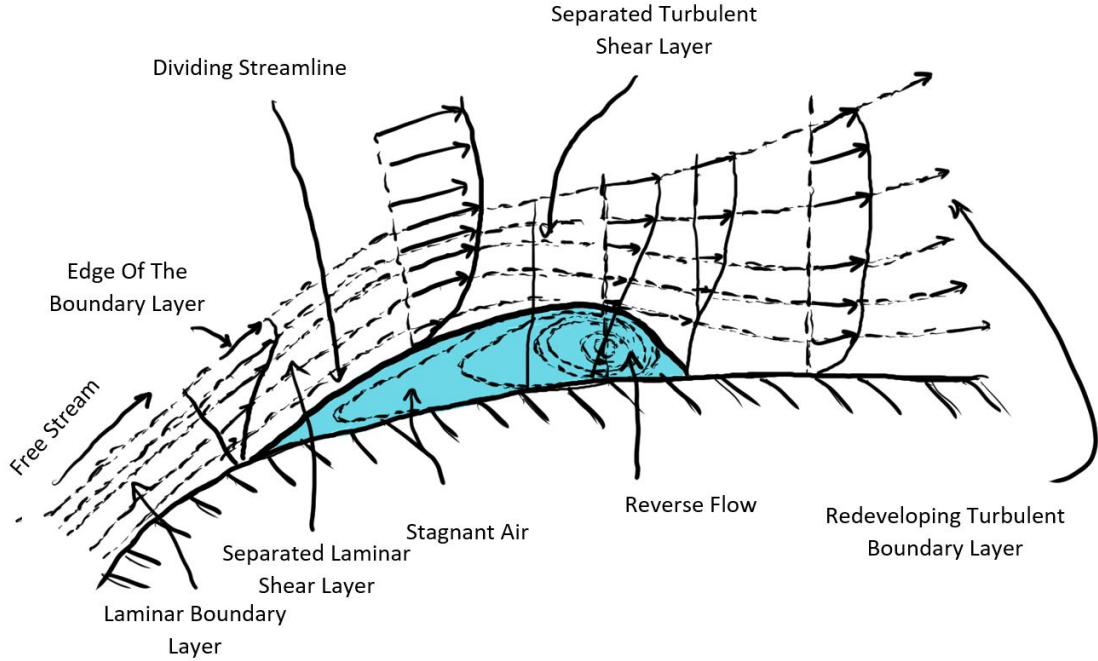


Fig. 3.4 Anatomy of laminar separation bubbles. Figure adapted from Mohamed [20]

Crini then investigated the implications of this separation when varying the angle of attack. Crini determined that the angle of attack of an airfoil affects the placement of LSBs. When the angle of attack suddenly increases (e.g. during a gust), a separation of the shear layer is also seen close to the leading edge [83]. Mohamed explains this as the shear layer transitioning earlier due to this disturbance [20]. Additionally, LSBs and vortices also significantly affect the coefficient of lift (C_L) of an airfoil. C_L is affected to a greater extent in smooth flow conditions as more suction is experienced inside an LSB with a smooth surface, as shown in Figure 3.5.

3.3 Low Reynolds Number Effects

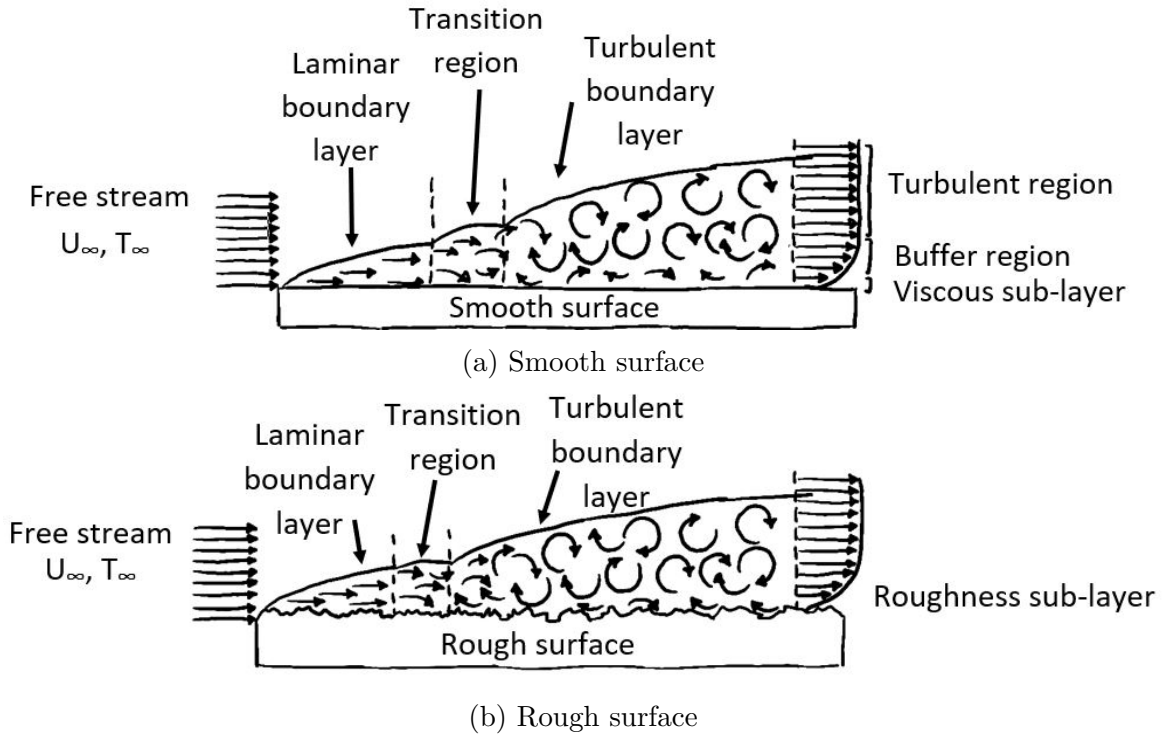
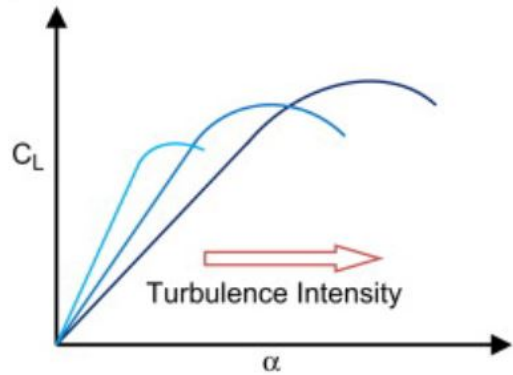


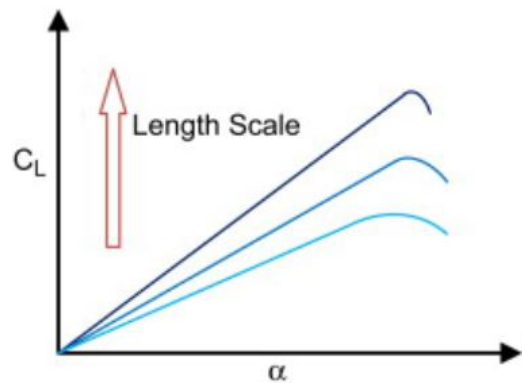
Fig. 3.5 a) Laminar flow to turbulence without surface roughness. b) Smaller transition region and turbulent boundary layer length with a rough surface. Figure is adapted [21].

Mohammed found this larger suction seen on smooth surfaces and induces pitching and rolling moments [20]. In the stall region angle of attack, turbulent flow results in a higher lift. The opposite is true for smooth flow. Turbulence could therefore increase the characteristic airfoil performance at low Reynolds numbers [20]. These characteristics are also shown in Figure 3.6.

Literature Review



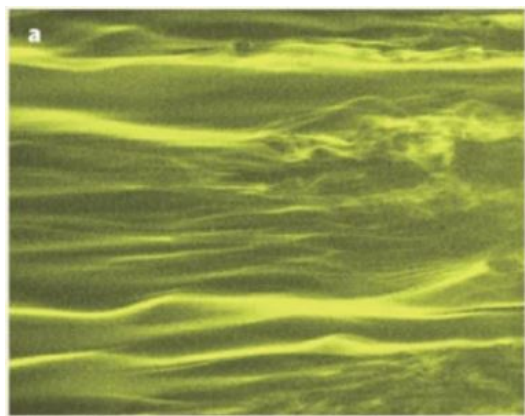
(a) Turbulence Intensity with lift curve



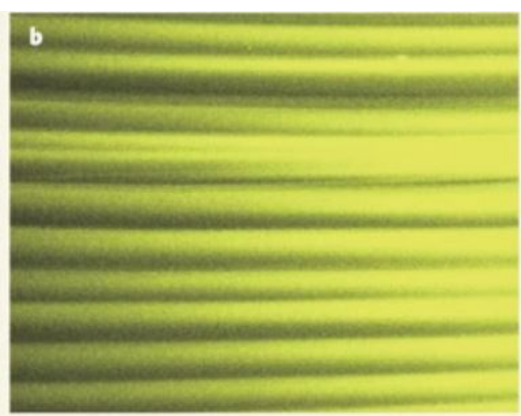
(b) Length scale with lift curve

Fig. 3.6 Airfoil aerodynamic performance variation with increasing: (a) turbulence intensity (b) length scale [20]

Investigations using materials with varying roughness have also been used to induce this transition to turbulent flow. Choi investigated this transition with some results shown in Figure 3.7. These show that the LSBs are reduced in the flow over airfoils when moving over a rough surface.



(a) Smooth surface



(b) Rough surface

Fig. 3.7 Flow patterns shown by smoke. Laminar flow to turbulence without surface roughness (a). Laminar flow for with a rough surface (b). [21]

3.3.2 Non-Linear Lift Distribution

Early on in the study of aerodynamics, theories developed from the study of conventional aircraft were applied to the bodies of small flying objects and animals such as birds. Traditional aerodynamic theories provide good results and insights when steady flows move across a stationary body. As mentioned by Roccia, they could not however, explain what allows small insects and birds to fly, leading to the paradox of "a bee cannot fly" [84] [85]. Roccia determined that the issue lies in the fact that non-linear and steady flows mainly characterize the flight of biological creatures [85]. This non-linear lift distribution is primarily caused by the low Reynolds number that these small bodies fly at and the low AR that MAV aircraft typically have ($AR < 3$).

Early experimental conducted by Winter showed that wings with small ARs can be described with a bound vortex flow and a wing-tip flow, which is also known today as vortices [86]. Wingtip vortices are particularly important, and even in general aircraft, lead to regulations such as spacing rules between aircraft and aerodynamic noise [87]. At the wingtips the pressure difference between the upper and lower surface cause a swirling vortex when in a free stream flow. This phenomenon is also shown in Figure 3.8. Cosyn and Vierendeels showed that this creates a low pressure cell at the wing tip which deforms the lift distribution in this region [78].

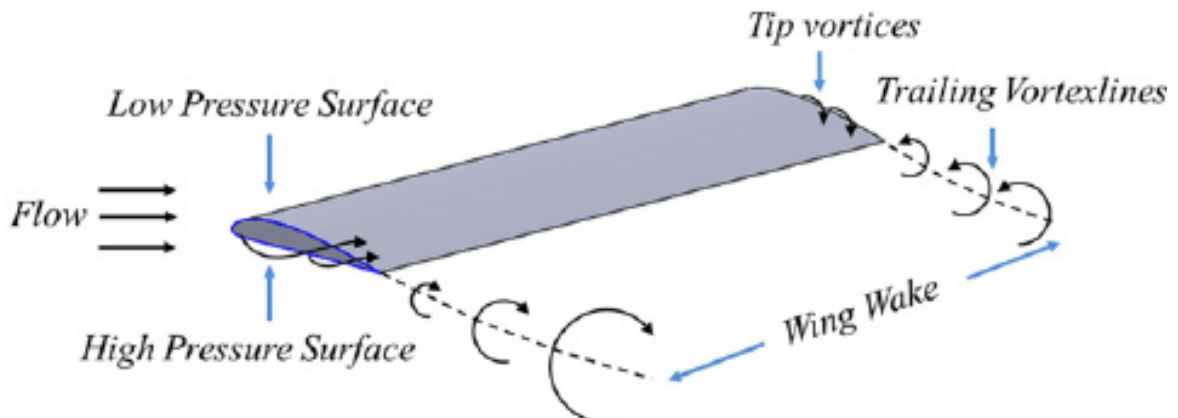


Fig. 3.8 Development of wingtip vortices over a wing section [22]

Literature Review

Zimmerman showed that the wing-tip geometry influences the aerodynamic performance for low AR wings [88]. Zimmerman also concluded that in order to produce the same coefficient of lift for lower AR wings, a higher angle of attack is required [88]. Low AR wings are also more susceptible to instability caused by disturbances [89]. Watkins showed that a sideslip is easily induced by a slight wind gust for low AR aircraft [90]. Shields investigated the inherent stability modes of low AR wings, determining that low AR wings have near-zero roll damping [91]. This means that roll moments created by flow asymmetries have a significant impact on low AR aircraft [91].

Mueller and DeLaurier found that for low AR aircraft, the center of lift was also sensitive to the angle of attack [92]. This is due to the wingtip vortices increasing with angle of attack. Therefore the non-linear aerodynamics dominate more at higher angle of attack, Pelletier also determined that these effects are more pronounced for low AR aircraft [93].

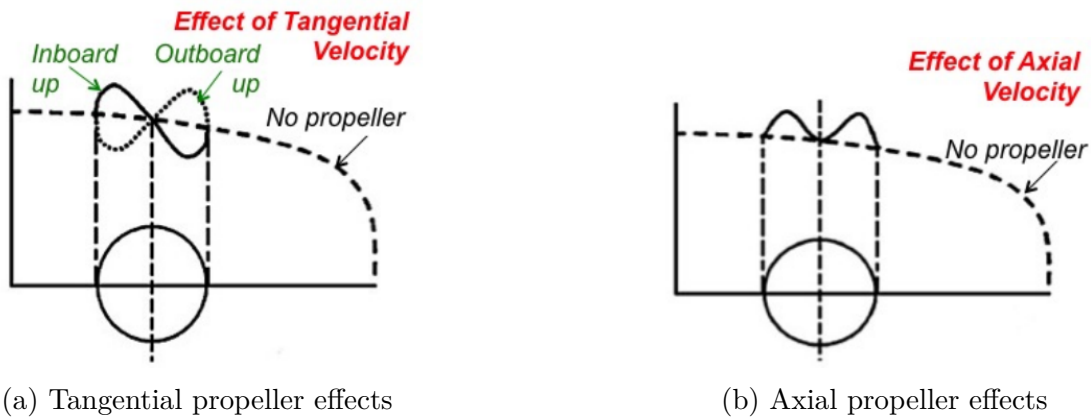
3.4 Propeller Wing Interaction

Propellers are commonly mounted on wings and significantly alter the flow seen over airfoils. Prandtl first studied the propeller-wing interaction at the start of the last century. The results concluded that two main effects impact the wing and flow behaviour. The first is due to the swirling of the propeller, which creates an ever-varying velocity. The second is due to an increase in inflow velocity [94]. Mounting propellers on the tips of the wing has also been shown to have benefits to performance compared with other wing positions [95]. Miranda found that substantial performance can be achieved by properly mounting propellers on the wingtips of wings [95], this was also further validated by Sinnige [96] and other teams [97] [98].

Numerical analysis by Rizk using the Vortex Lattice Method has also validated these observations [99]. Veldhuis foundn that propellers have a higher axial velocity at the

3.4 Propeller Wing Interaction

blade tip than where it is joined at a hub [97]. Ferraro also determined that the slipstream created by the propeller can be split into the axial, and tangential velocity components [23]. The tangential velocity component accounts for the dynamic pressure across the wing [23]. The swirl is anti-symmetrical and changes the incoming flow that the wing sees. This is also shown in Figure 3.9(a) [23]. The axial velocity affects the dynamic pressure on the wing. The axial velocity is considered to be symmetric when the propeller flow is uniform and undisturbed, as shown in Figure 3.9(b) [23].



(a) Tangential propeller effects

(b) Axial propeller effects

Fig. 3.9 Tangential and Axial velocity effects [23]

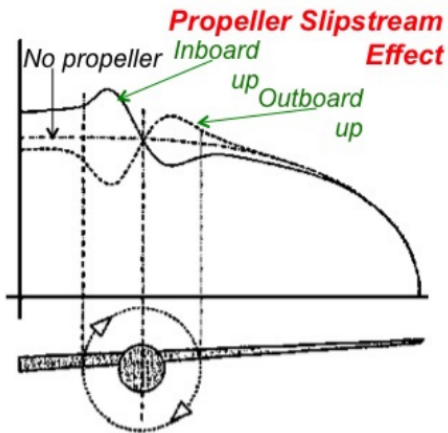


Fig. 3.10 Propeller slipstream effects on a finite wing [23]

As the dynamic pressure increases, a gain in lift coefficient is seen as shown in Figure 3.11. This increase in lift coefficient is also partially due to the lack of separation seen

Literature Review

when increasing the revolutions per minute (RPM) of the propeller. Shams shows that this leads to a forward shift in the aerodynamic center of the aircraft [68] [66].

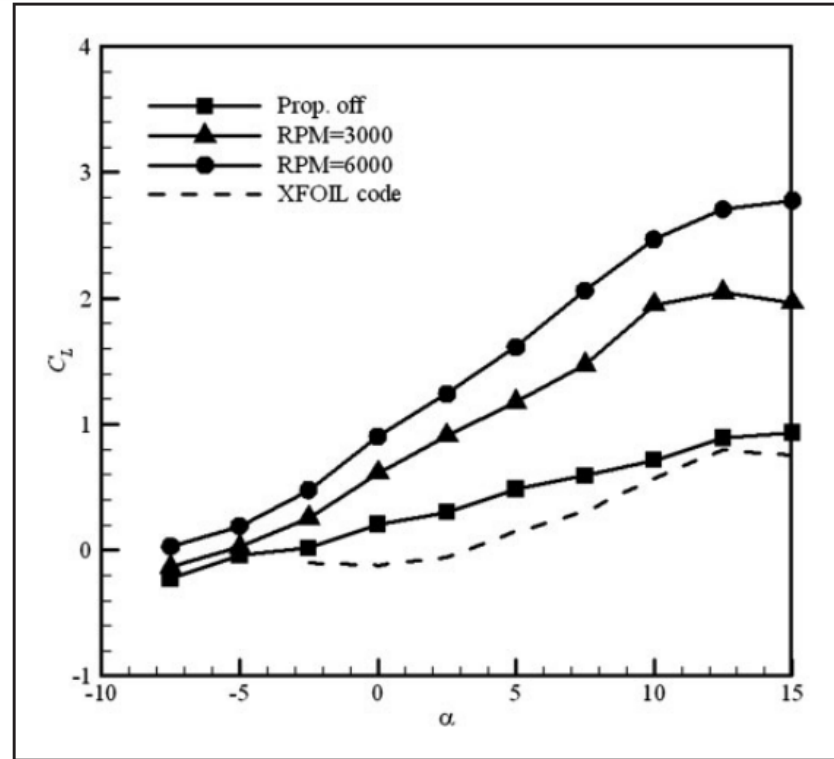


Fig. 3.11 Effect of propeller slipstream on the lift coefficient curve with angle of attack ($Re = 0.3 \times 10^5$) [24].

The slipstream effect is shown in Figure 3.12. The inboard wing sees a higher angle of attack, and hence an up-wash effect is seen ($y/b > 0$). Aminaei found that in the propeller down-wash region ($y/b < 0$) a delay is experienced in the flow transition than when compared with the up-wash region [24]. This is due to the reduced local angle of attack on the wing, which moves the transition region towards the trailing edge. These effects can also affect the flow stream beyond the propeller and lead to non-linear lift distributions further from the propeller as well.

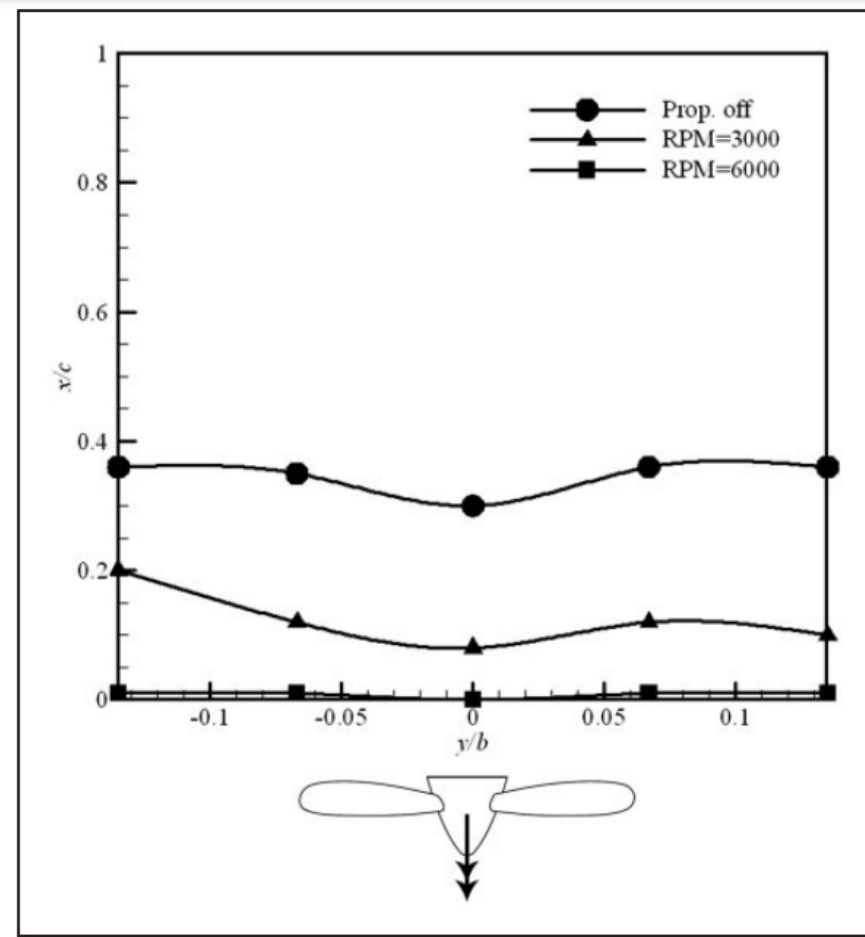


Fig. 3.12 Propeller slipstream effect with span-wise location for airflow transition over the wing upper surface, $\alpha = 2.5^\circ$ [24].

Prantl was one of the first to investigate the influence of propellers on wings [100] and Franke and Weinig one of the first to investigate the rotational velocity's effects on the lift distribution across the wing [101]. Framk and Weinig showed that the circulation distribution in regards to the slipstream can be predicted and used the lifting line theory in order to prove this [101]. Jameson went on to develop simple equations to quantify the lift and drag of wings in jet slipstreams [102]. Ellis developed programs to run multiple lifting line approximations in order to quantify the circulation pattern, when propeller effects are being accounted for [103]. These approximations however, were all too rudimentary and could not be used to predict the flow characteristics

Literature Review

over wings. Several models and equations to represent these effects have been created. Veldhuis concluded that the propeller effects can only be described completely when using the Full Interaction Mode (FIM) [25].

Veldhuis also determined that there are four main regions of influence which the propeller has. These proposed sections are not independent of each other but rather act as a smooth transition from one to the other [25]. As shown in Figure 3.13 the local blade angle of attack increases where the blade move down (P-II in Figure 3.13) and decreases where the blade moves up (P-IV in Figure 3.13). The induced angle of attack is visualised in Figure 3.14. The effect of the propeller to induce this change in effective angle of attack is most greatly seen when the propeller is parallel to the wing span [25].

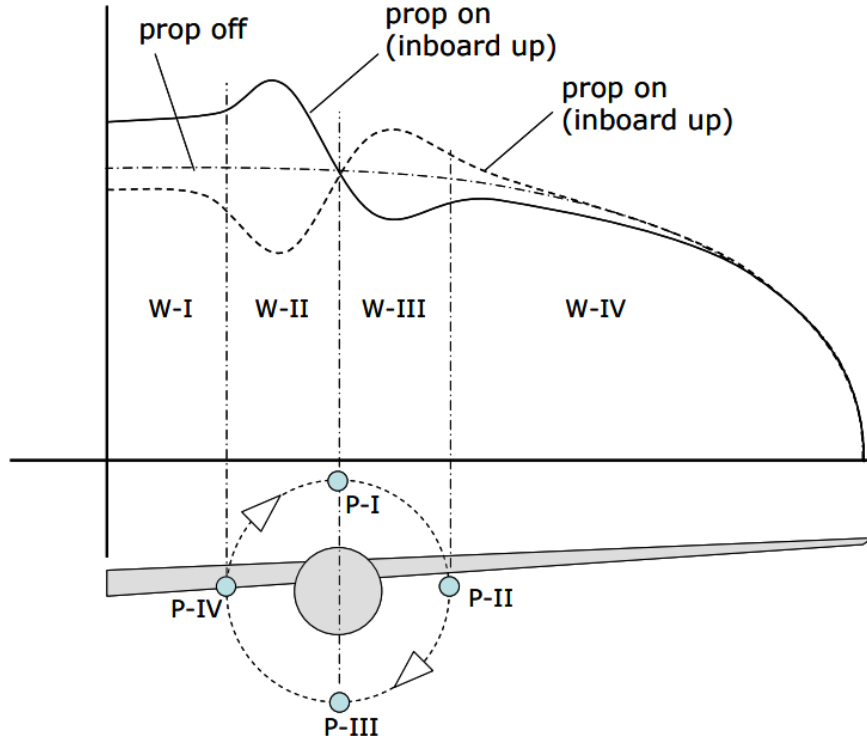


Fig. 3.13 Influence areas related to propeller-wing interaction based on the loading distributions [25]

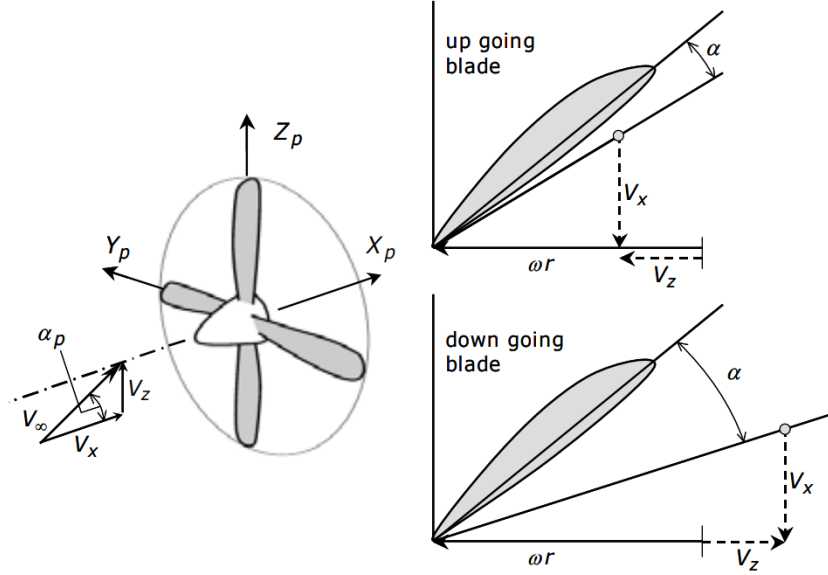


Fig. 3.14 Blade angle of attack variation due to propeller pitch angle [25]

Velhuis also found that the extent of the swirl relaxation is dependent on the propellers position, free stream conditions and the overall wing loading [25]. A more recent study by Velhuis simulated these effects through the use of CFD [104]. Ananda also concludes that for the tractor configuration, in a low speed wind tunnel, the flow transitions to turbulent flow earlier. This reduces the drag and increases the lift to drag ratio. These benefits were not seen when analysing the pusher configuration.

3.4.1 Stability Effects

As propellers have been shown to have a strong influence on the lift distribution across wings, the overall lateral and longitudinal stability will be affected. Shams has showed that increasing the propeller diameter and RPM increase the moment produced creating a larger pitching moment on the aircraft [68]. Tractor configurations have also been investigated by Shams. The tractor configuration creates an increase in the rolling and

Literature Review

yaw moments acting on the aircraft [68]. Propellers do also produce a torque effect, further destabilizing the aircraft by creating an asymmetric roll.

3.4.2 Aerodynamic Parameters

The characteristics of an aircraft are given by a combination of the aerodynamic parameters that describe it. For MAV, this is more complex as these aircraft do not allow for the same assumptions to be made in calculations. New methods such as those developed by Shen, for determining the aerodynamic parameters are currently being developed, and proposed in order to address these differences [105] [106]. Aerodynamic forces are crucial to the overall design of any aircraft [107]. In order to determine these forces for MAVs, a variety of techniques have been used, such as the Athena Vortex Lattice Method used by Stewart and Hrad [26] [108]. However, this method cannot predict the separation of flow as the lift is assumed to increase linearly with the angle of attack. This is not the case at low Reynolds numbers [109]. Aboelezz outlines a process in which a fixed-wing MAV can be designed, whereby he uses physical wind tunnel testing in order to evaluate the MAVs actual flight performance [42]. Bollay and Belotserkovskii have both proposed modified versions of Prandtl's lifting line theory [110] [111], though validations with experimental data are limited in scope and do not validate propeller-wing interactions.

3.4.3 The General Micro Aerial Vehicle

Today the interest, research and development of MAVs are continually increasing. However, in order to focus on particular aspects or compare various designs, a "baseline" geometry is required. An example of this is the GENMAV developed by Stewart[26] shown in Figure 3.15.



Fig. 3.15 GenMAV Model [26]

While there are various models which have been tested to determine the main aerodynamic properties [26] [42], none have completed a physical wind tunnel test while accounting for the effects of a powered propeller. Initial GENMAV aerodynamic data was determined by using the vortex-panel method by Stewart[26], and did not involve wind tunnel testing. The effects of propeller induced flow have also been studied for both fixed and free-spinning propellers, but currently, no data is available for wind tunnel tests of a powered propeller MAV.

3.4.4 Optimization Techniques and Validation

Many non-standard aircraft designs are evaluated using software in order to analyse aerodynamic characteristics and then optimised through a variety of typical software engineering methods such as the particle swarm method used by Gomez to optimize the algorithm for the attitude and altitude and Boutemedjet who used this to optimize the wing planform parameters of a MAV [112] [113]. These procedures are used, as non-standard aircraft designs are more tedious to design and even more complex to set

Literature Review

up and test than standard aircraft designs. The unique constraints that MAVs have and how they led to poor attitude control are shown in Figure 3.16.

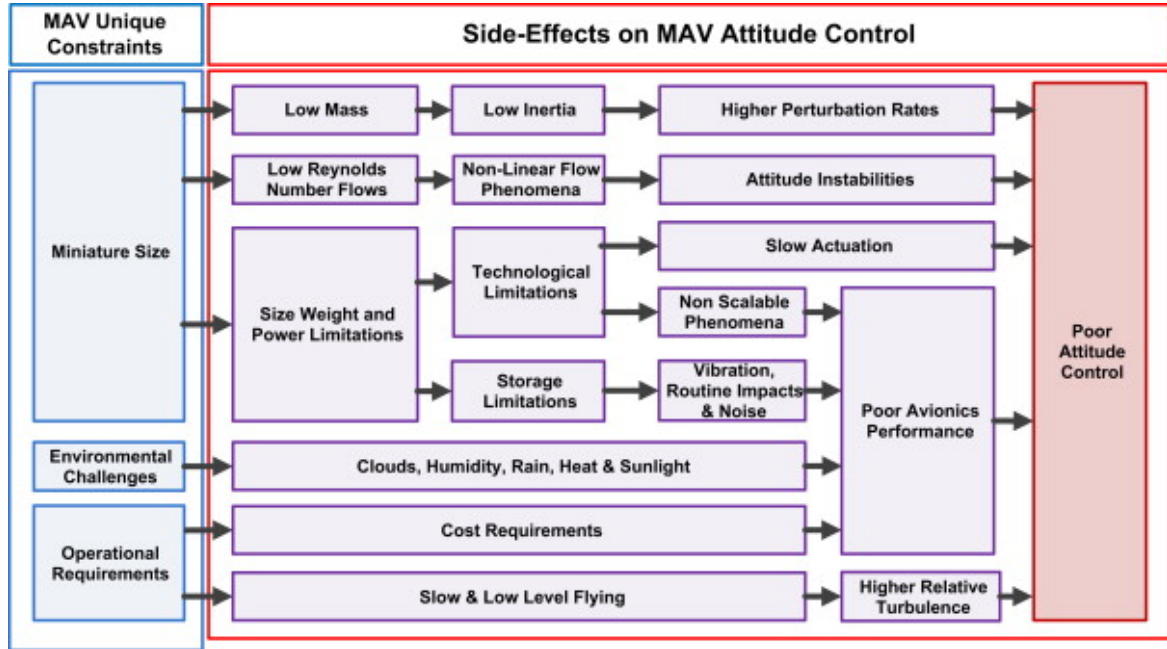


Fig. 3.16 Unique constraints of MAVs [20]

Mohamed found that the physical size, environment and flight regime have strong effects on a MAVs ability to fly and carry payloads [20]. Many groups of researchers have created software to optimize MAVs by using optimization algorithms such as genetic algorithms, non-dominating sorting generic algorithms, particle swarm optimization and sequential quadratic optimization programs. While some have accounted for low speed flight [40] [61] [62], no optimization techniques accounting for propeller-interaction effects currently exist. Many investigations into propeller effects show the propeller has significant effects on wing aerodynamics, both in regards to performance and also stability [114] [115]. None have been used with the results of free-flowing propellers in physical wind tunnel testing. Therefore these software models are currently invalid when also accounting for propeller-wing effects.

Chapter 4

Theory and Methodology

This chapter outlines the theory and Methodology used create, test and collect the data required for the wing-propeller interaction analysis.

4.1 Material Choice

In order to readily edit and modify the model to be tested 3D printing was used to print the final developed model. 3D printing has become increasingly common when developing models to be testing in wind tunnels. Polyatic acid (PLA) filament was used to print the main body of the model as this is the most widely used and available filament for 3D printing purposes. It has a reasonably low melting point of ≈ 150 °. good layer adhesion and. It can also be extruded in a variety of ways in order to develop different textures on the surface of the 3D model. This is particularly significant for MAVs as the surface of aircraft are typically smooth in order to reduce viscous drag effects. 3D printed models often have ridges between layers which have been printed.

However

interrogate
Ben

4.2 FreeCAD

FreeCAD is a 3D parametric modeler and was used with provided python scripts to produce fuselage, wing and tail shapes when given input parameters to define the shape and geometry. Various model shapes were produced with the aim of making the model 3D printable in order to allow for ease of manufacturing and testing. Several design constraints had to be considered when developing the model due to the structural strength of the PLA used for 3D-printing and the limitations . the wings and tail could

not be

The model was also fitted to mount into the 3x4 wind tunnel for testing as shown in figure here

4.3 VAP 3.5

VAP 3.5 is a open-source software which uses the High-Order Free Wake (HOFW) method in order to determine the aerodynamic performance of MAV designs.

The HOFW method

4.4 XFOIL

XFOIL is another open source free to use software which has been developed by Harold Youngren and Mark Drela. The software is used to analyse 2D airfoils for their aerodynamic characteristics. XFOIL was used to produce aerofoil data which accounted for viscous effects. It is essential that the software account for the viscous

4.5 Model Development

effects as this has an essential role in the flow characteristics across the surface of an aircraft wing. This is especially true at low Reynolds numbers where the [XFOIL](#) finsih this accounts for the viscous effects by using the wake momentum thickness to determine the skin friction produced as fluid passes over the surface of the airfoil as given by Equation 4.1.

$$\theta = \int_0^\infty \frac{u}{U_e} \left(1 - \frac{u}{U_e}\right) dy \quad (4.1)$$

Where:

- θ is the momentum thickness at a given point along the airfoil
- U_e is the freestream velocity
- u is the flow velocity at a position y distance from the airfoil surface

In this manner the skin friction losses can be determined and accounted for when running the VAP software to analyse the stability of the model.

4.5 Model Development

4.6 Wind Tunnel Testing

In order to analyse the stability of the final developed model in the three configurations, the model was mounted in the wind tunnel to determine the forces and moments acting at several conditions in order to assess the effect that adding a propeller has on the stability of the model

Theory and Methodology

4.6.1 Wind Tunnel Setup

Wind tunnel tests were taken for several variations of Ao_a, airspeed, propeller speed and configuration. These are outlined below

- Ao_a: -5 ° to 15 ° in increments of 2°_{inc}
- Airspeed: 10m/s, 15m/s and 20m/s
- Motor speed: 6000RPM, 9000RPM, 11000RPM
- Configuration: No propeller, tractor and pusher

A safety net was placed in the wind tunnel in case any parts of the model were unable to remain attached as the airspeed increased to 20m/s.

The nano25 load cell was used to record the forces and moments acting on the model about the mounting position at 25 \bar{c} .

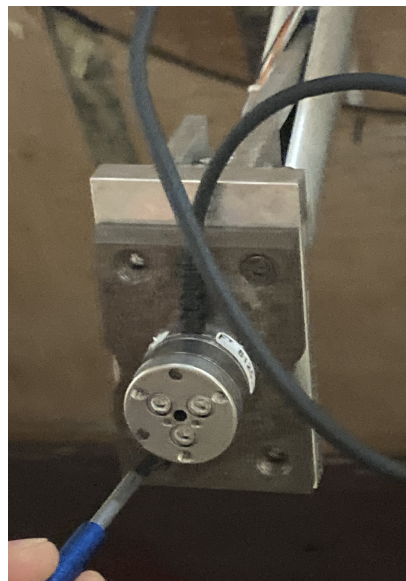


Fig. 4.3 Nano 25 load cell mount

4.6 Wind Tunnel Testing



Fig. 4.1 Safety net to

The model mount was then attached over the load cell.

The model was then attached in three main configurations. These were mounting the propeller without a propeller, in a tractor and pusher configurations.

The wind tunnel was then calibrated for wind speed, atmospheric conditions and angles of attack. The mount used for the model was double checked using a pitch gauge to ensure the angle of attack was correct.

When using the prop the motor was supplied with a 7.4V battery and the RPM was set to $\approx 6000RPM$, $\approx 9000RPM$ and $\approx 11000RPM$.

Theory and Methodology



Fig. 4.2 Caption

4.7 Stability Calculation

In order to determine the stability of the model in all the tested configurations the stability derivatives of the model had to be determined. Data from the nano 25 load cell was used to determine the loads and moments acting on the model about the mounting point. These values were transformed to the neutral point of the model at $20\bar{c}$. The aerodynamic coefficients were determined using equations 2.5 to 2.6 and the moment

4.7 Stability Calculation



coefficients about the pitch, yaw and roll axis were calculated using Equations 2.10 to 2.13.

Theory and Methodology



Fig. 4.4 Examples of MAVs with category

4.7 Stability Calculation

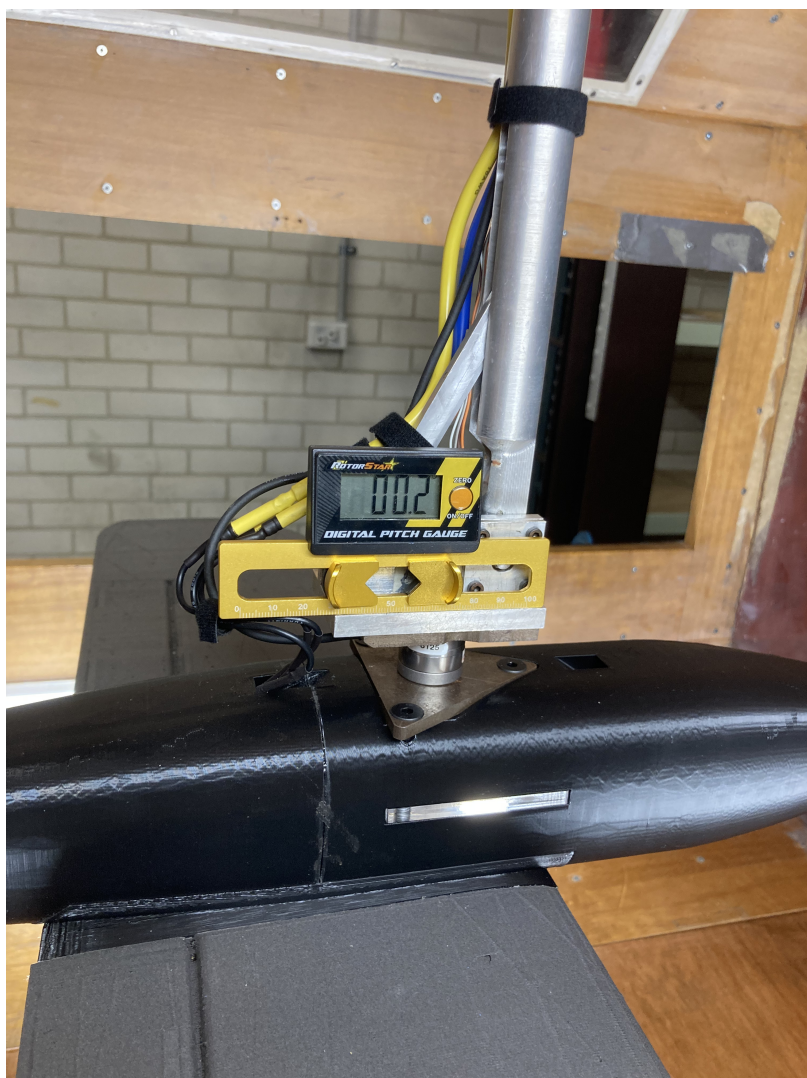


Fig. 4.5 Calibrating pitch of model mount to ensure Aoa is accurate

Chapter 5

Results and Discussion

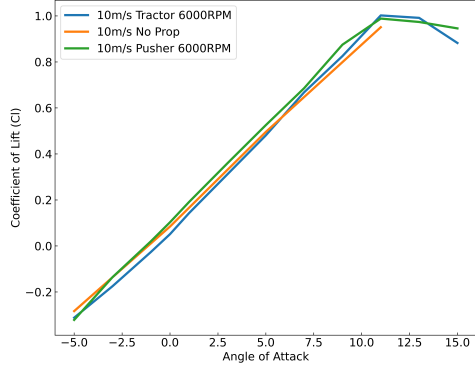
5.1 Wind Tunnel Results

Wind tunnel

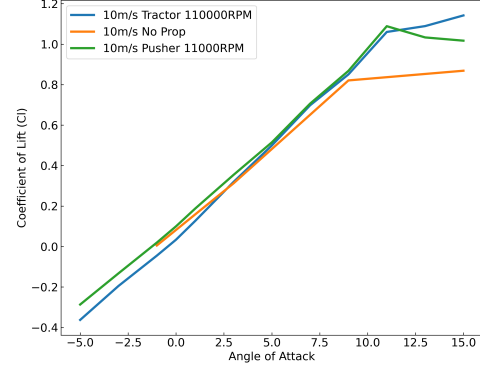
5.1.1 Aerodynamic Coefficient of Lift

fig. 5.1(a) and fig. 5.1(b) show that as the motor speed increases from 6000RPM to 11000RPM the co-efficient of lift increases slightly for both the tractor and pusher configurations. The lift curve also does not drop off as typically seen in aircraft. The tractor configuration sees an increase in the lift coefficient beyond the stall point while the pusher configuration has a linear decrease in the lift coefficient beyond the stall point. Increasing the airspeed dramatically decreases the lift coefficient. This is seen at all motor speeds and is shown between fig. 5.1(a) and fig. 5.1(c) as well as between fig. 5.1(b) and fig. 5.1(d)

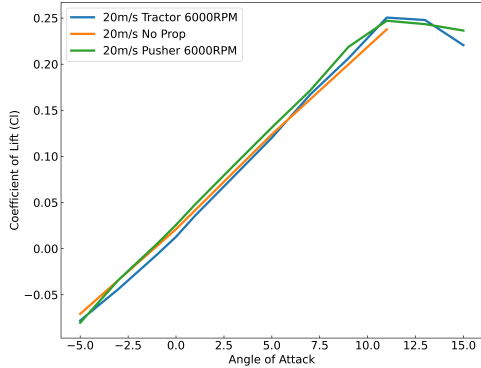
5.1 Wind Tunnel Results



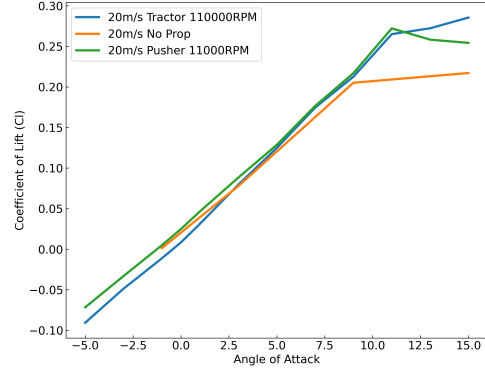
(a) Coefficient of lift at 10m/s airspeed and 6000RPM motor speed



(b) Coefficient of lift at 10m/s airspeed and 11000RPM motor speed



(c) Coefficient of lift at 20m/s airspeed and 6000RPM motor speed



(d) Coefficient of lift at 20m/s airspeed and 11000RPM motor speed

Fig. 5.1 Coefficient of lift variation with various conditions for the pusher, tractor and no propeller configurations

5.1.2 Aerodynamic Coefficient of Drag

Figure 5.2 shows that as the airspeed of the wind tunnel increased the coefficient of drag shifted upwards for both the pusher and tractor configuration. The drag for both the tractor and puller configuration at 10ms^{-1} airspeed is negative and indicates that the drag on the MAV model is being reduced with the addition of the propeller to the MAV model. The highest coefficient of drag is seen when no propeller is operating on

Results and Discussion

the MAV model. When no propeller is added, no significant changes are seen with airspeed for the coefficient of drag. The tractor configuration in general reduces drag compared with the pusher configuration, this is most clearly seen at 20ms^{-1} in Figure 5.2. As the airspeed increases the coefficient of drag is also seen to increase for the pusher and tractor configuration.

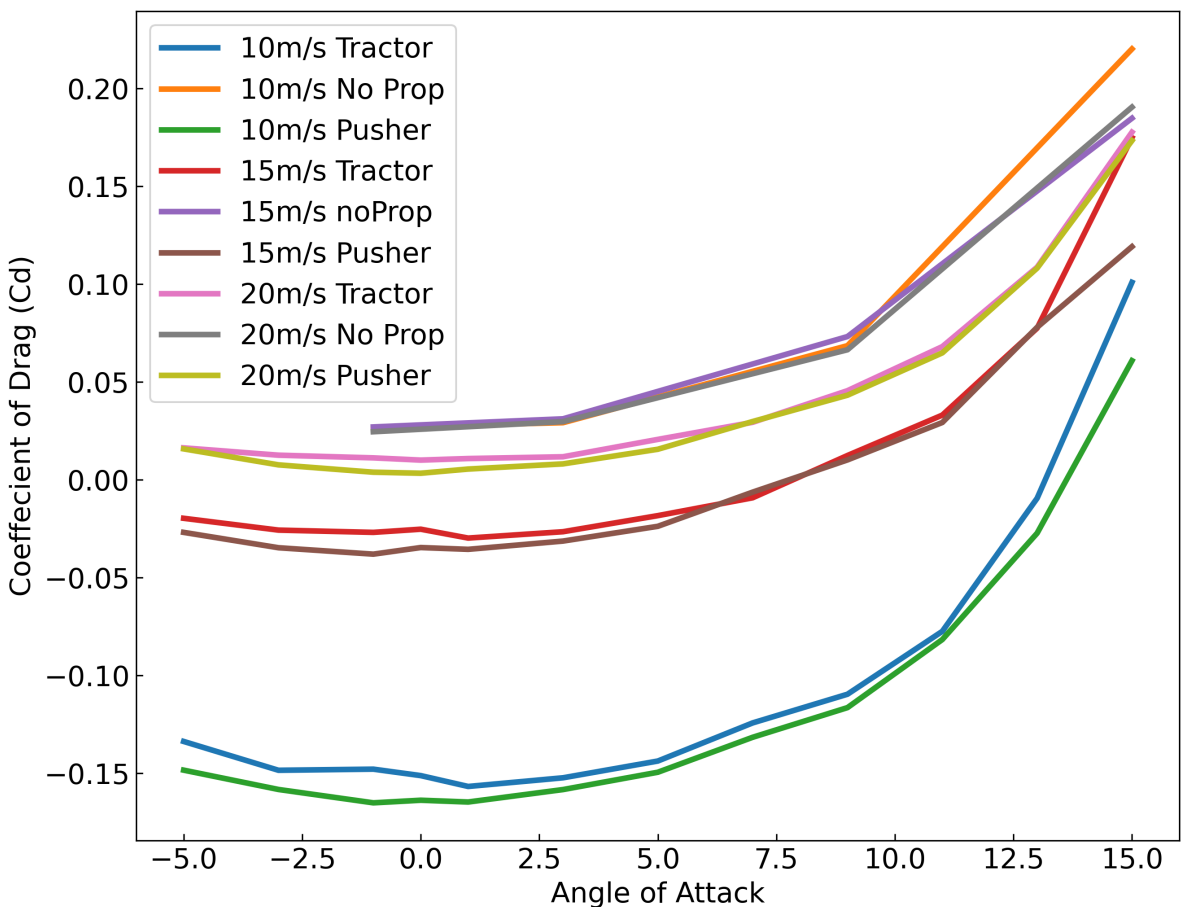


Fig. 5.2 Coefficient of drag variation at 11000RPM motor speed for the tractor, pusher and no propeller configurations

Figure 5.3 shows minimal differences between the pusher and tractor configurations. The addition of the propeller increases drag at 6000RPM, however as the motor speed

5.1 Wind Tunnel Results

increases to 11000RPM there is a significant drop in the coefficient of drag for both the tractor and pusher configuration.

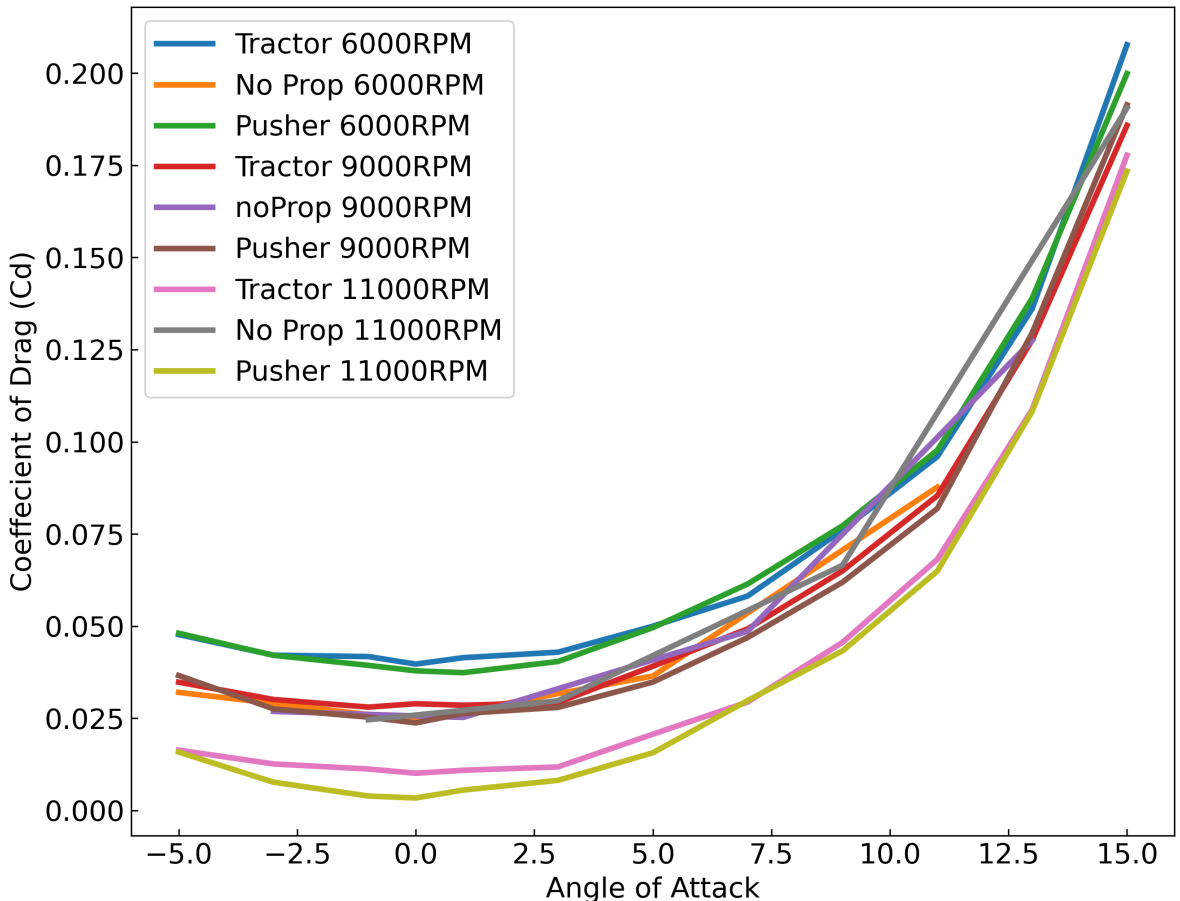
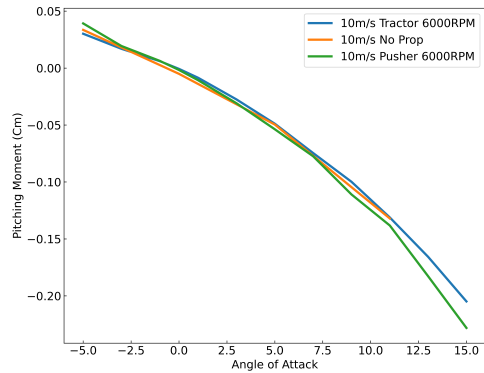


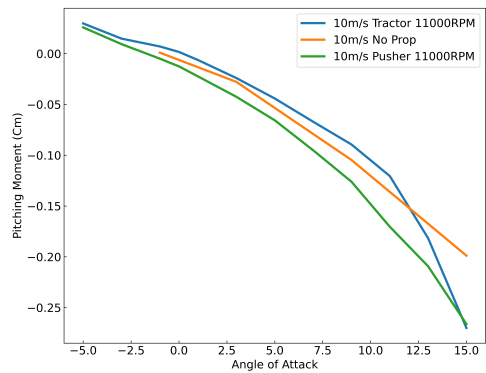
Fig. 5.3 Coefficient of drag variation at 20ms airspeed for the tractor, pusher and no propeller configuration

Results and Discussion

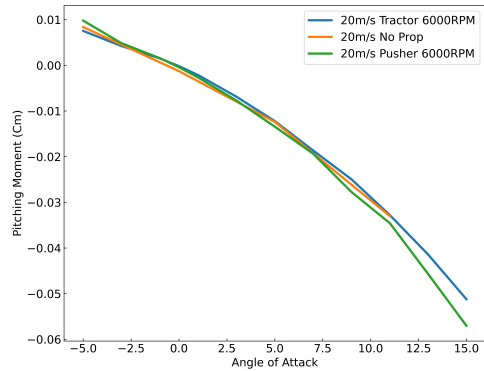
5.1.3 Pitching Moment Coefficient



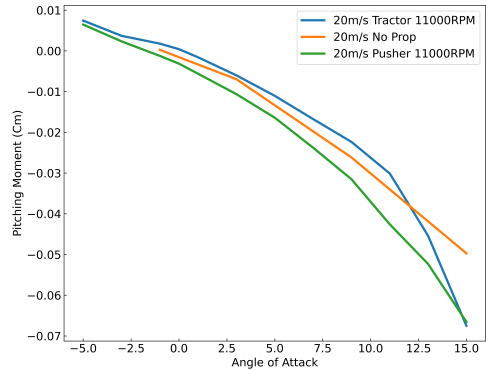
(a) Pitching Moment Coefficient at 10m/s airspeed and 6000RPM motor speed



(b) Pitching Moment Coefficient at 10m/s airspeed and 11000RPM motor speed



(c) Pitching Moment Coefficient at 20m/s airspeed and 6000RPM motor speed



(d) Pitching Moment Coefficient at 20m/s airspeed and 11000RPM motor speed

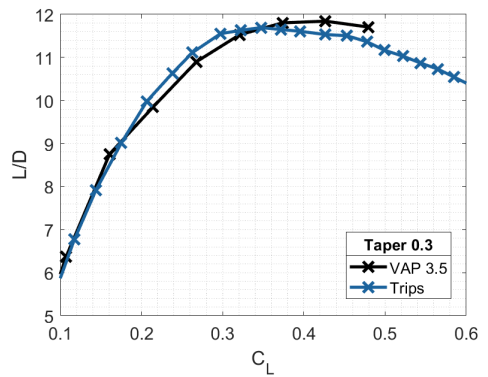
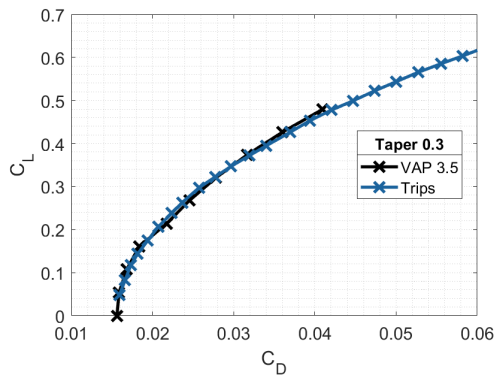
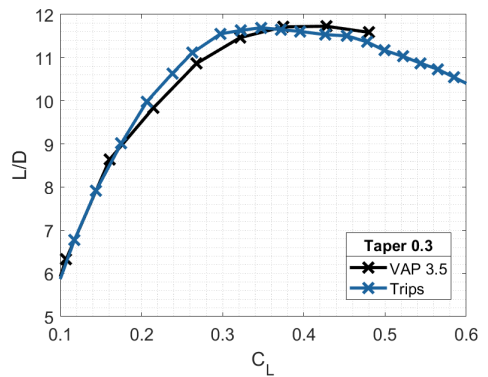
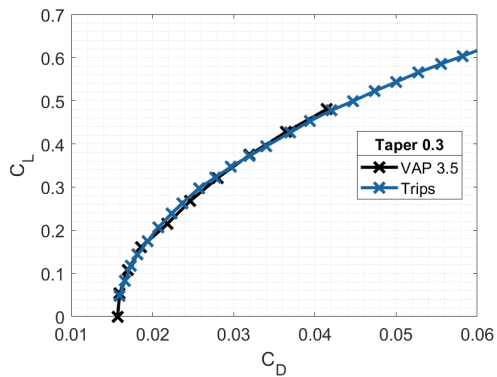
5.1.4 Yawing Moment Coefficient

5.1.5 Rolling Moment Coefficient

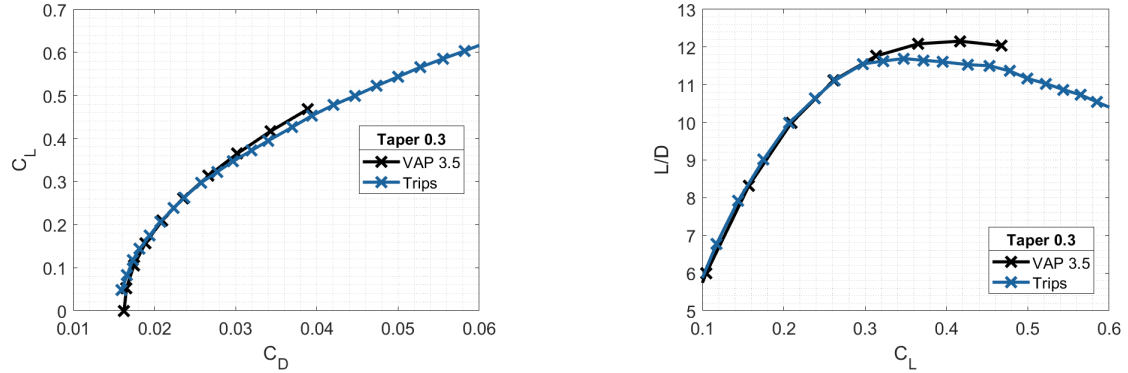
5.1.6 Static Margin

5.2 VAP Validation

5.2.1 Wing Validation



Results and Discussion



5.2.2 Model Validation

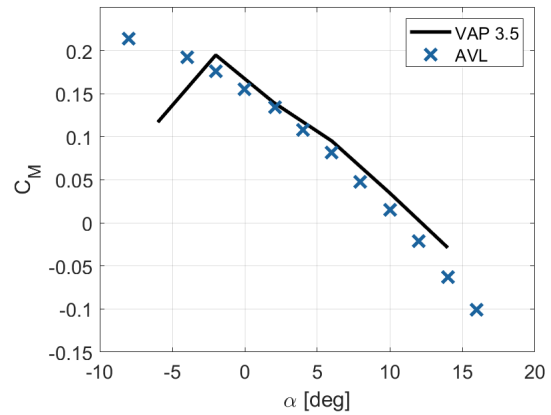
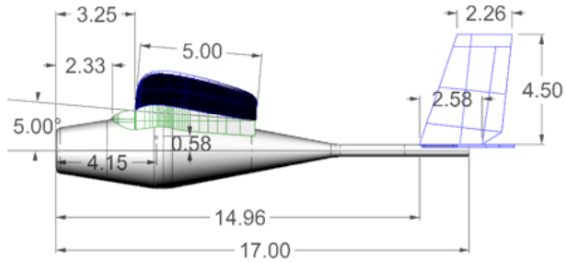


Fig. 5.11

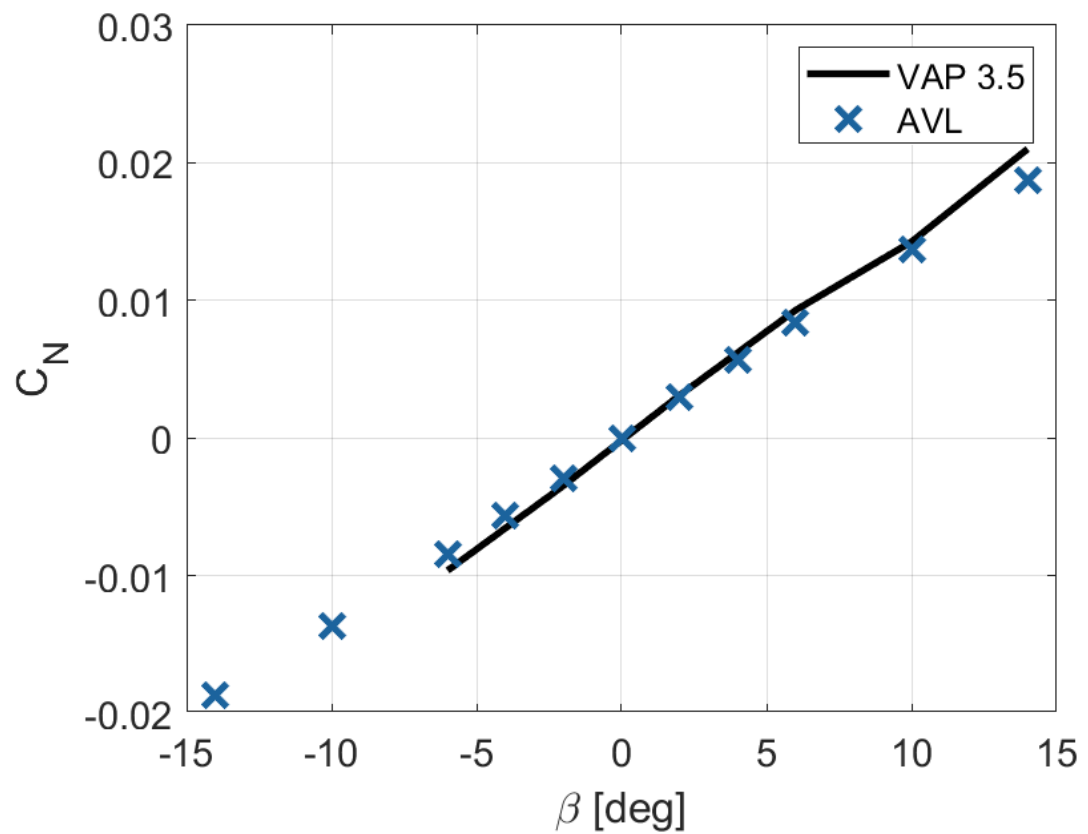


Fig. 5.13

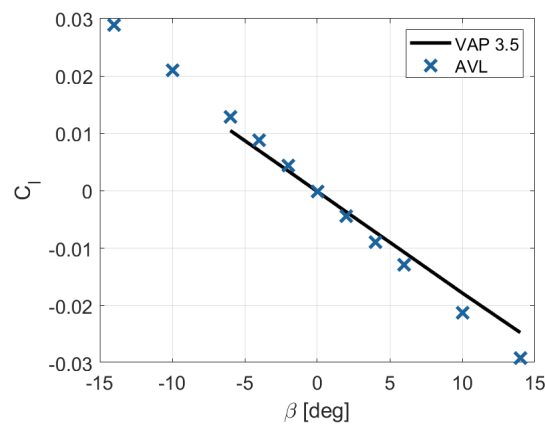


Fig. 5.12

Results and Discussion

5.3 Discussion

References

- [1] Zakaria Mohamed Yehia, Moatassem Abdallah, and Adnan Elshaafi. Classification of uavs with respect to size and weight | download scientific diagram, 2012. URL https://www.researchgate.net/figure/Classification-of-UAVs-with-respect-to-size-and-weight_fig1_312115495.
- [2] Micro-air-vehicle enviroment system | projects | research & production | digital worlds institute | college of the arts | university of florida, 2022. URL <https://digitalworlds.ufl.edu/research-production/projects/micro-air-vehicle-enviroment-system/>.
- [3] World's first hummingbird-like unmanned aircraft system takes flight, 2011. URL <https://newatlas.com/aerovironment-nano-hummingbird/17918/>.
- [4] K. Dalamagkidis. On integrating unmanned aircraft systems into the national airspace system. *Intelligent Systems, Control and Automation: Science and Engineering*, 36, 2009.
- [5] Roberto Sabatini, Subramanian Ramasamy, Alessandro Gardi, and Leopoldo. Rodriguez Salazar. Low-cost sensors data fusion for small size unmanned aerial vehicles navigation and guidance., 2013. URL https://www.researchgate.net/figure/AEROSONDE-UAV-characteristics-Adapted-from-25_fig3_263970095.
- [6] Hunter rq-5a / mq-5b/c uav - army technology, 2021. URL <https://www.army-technology.com/projects/hunter/>.
- [7] Iai rq-2 pioneer, 2022. URL https://www.militaryfactory.com/aircraft/detail.php?aircraft_id=325.
- [8] Mq-9 reaper uav (cropped) - general atomics mq-9 reaper - wikipedia, 2022. URL [https://en.wikipedia.org/wiki/General_Atomics_MQ-9_Reaper#/media/File:MQ-9_Reaper_UAV_\(cropped\).jpg](https://en.wikipedia.org/wiki/General_Atomics_MQ-9_Reaper#/media/File:MQ-9_Reaper_UAV_(cropped).jpg).
- [9] Japan's first global hawk begins flying at northrop's california drone hub, 2021. URL <https://www.defensenews.com/global/asia-pacific/2021/04/19/japans-first-global-hawk-begins-flying-at-northrops-california-drone-hub/>.
- [10] Nasa armstrong fact sheet: X-29 advanced technology demonstrator aircr | nasa, 2015. URL <https://www.nasa.gov/centers/armstrong/news/FactSheets/FS-008-DFRC.html>.

References

- [11] (139) pinterest, 2022. URL
<https://www.pinterest.nz/pin/317644579972770591/>.
- [12] Reference frames and how they are used in inertial navigation · vectornav, 2022. URL <https://www.vectornav.com/resources/inertial-navigation-primer/math-fundamentals/math-refframes>.
- [13] Noor Iswadi Ismail. Aerodynamic performances of twist morphing mav wing, 2015. URL https://www.researchgate.net/figure/Reynolds-number-operation-for-different-aircraft-vehicles-2_fig1_280534123.
- [14] Butterfly definition and meaning | collins english dictionary, 2022. URL
<https://www.collinsdictionary.com/dictionary/english/butterfly>.
- [15] Pheasant stock photos, royalty free pheasant images | depositphotos, 2022. URL
<https://depositphotos.com/stock-photos/pheasant.html>.
- [16] Light aircraft 2-lateral view white background 3d rendering ilustracion 3d stock illustration - illustration of technology, isolated: 231762604, 2022. URL
<https://www.dreamstime.com/d-render-illustration-air-transport-airplane-plane-aviation-light-aircraft-lateral-view-white-background-rendering-ilustracion-image231762604>.
- [17] Jp scheinelier: Boeing 747-400., 2020. URL
https://twitter.com/jp_scheinelier/status/1274697589506490372.
- [18] Gavin K. Ananda, Michael S. Selig, and Robert W. Deters. Experiments of propeller-induced flow effects on a low-reynolds-number wing. *AIAA Journal*, 56: 3279–3294, 6 2018. ISSN 00011452. doi:
10.2514/1.J056667/ASSET/IMAGES/LARGE/FIGURE30.JPG. URL
<https://arc.aiaa.org/doi/10.2514/1.J056667>.
- [19] Justin Winslow, Hikaru Otsuka, Bharath Govindarajan, and Inderjit Chopra. Basic understanding of airfoil characteristics at low reynolds numbers (104–105). *Journal of Aircraft*, 55:1050–1061, 12 2018. ISSN 15333868. doi:
10.2514/1.C034415/ASSET/IMAGES/LARGE/FIGURE17.JPG. URL
<https://arc.aiaa.org/doi/full/10.2514/1.C034415>.
- [20] Abdulghani Mohamed, Kevin Massey, Simon Watkins, and Reece Clothier. The attitude control of fixed-wing mavs in turbulent environments. *Progress in Aerospace Sciences*, 66:37–48, 4 2014. ISSN 0376-0421. doi:
10.1016/J.PAEROSCI.2013.12.003.
- [21] Kwing So Choi. The rough with the smooth. *Nature* 2006 440:7085, 440: 754–754, 4 2006. ISSN 1476-4687. doi: 10.1038/440754a. URL
<https://www.nature.com/articles/440754a>.

References

- [22] Kumar Tufan. Development of wingtip vortices over a wing section | download scientific diagram, 2015. URL https://www.researchgate.net/figure/Development-of-wingtip-vortices-over-a-wing-section_fig1_277028223.
- [23] Giovanna Ferraro, Timoleon Kipouros, A. Mark Savill, Abdul Rampurawala, and Christian Agostinelli. Propeller-wing interaction prediction for early design. *52nd AIAA Aerospace Sciences Meeting - AIAA Science and Technology Forum and Exposition, SciTech 2014*, 2014. doi: 10.2514/6.2014-0564.
- [24] Hamzeh Aminaei, Mojtaba Dehghan Manshadi, and Ali Reza Mostofizadeh. Experimental investigation of propeller slipstream effects on the wing aerodynamics and boundary layer treatment at low reynolds number. *Proceedings of the Institution of Mechanical Engineers, Part G: Journal of Aerospace Engineering*, 233:3033–3041, 6 2019. ISSN 20413025. doi: 10.1177/0954410018793703.
- [25] L Veldhuis. Review of propeler-wing aerodynamics, 2004. URL http://icas.org/ICAS_ARCHIVE/ICAS2004/PAPERS/065.PDF.
- [26] Kelly Stewart, Jeffrey Wagener, Gregg Abate, and Max Salichon. Aiaa 2007-667. In *Design of the air force research laboratory micro aerial vehicle research configuration*, volume 12, 2007. doi: 10.2514/6.2007-667.
- [27] Xiao Feng Liu, Zhi Wei Guan, Yu Qing Song, and Da Shan Chen. An optimization model of uav route planning for road segment surveillance. *Journal of Central South University 2014* 21:6, 21:2501–2510, 6 2014. ISSN 2227-5223. doi: 10.1007/S11771-014-2205-Z. URL <https://link.springer.com/article/10.1007/s11771-014-2205-z>.
- [28] Sudhir Kumar Chaturvedi, Raj Sekhar, Saikat Banerjee, Hutanushu Kamal, and Corresponding Author. Comparative review study of military and civilian unmanned aerial vehicles (uavs). *INCAS BULLETIN*, 11:183–198, 2019. ISSN 2247-4528. doi: 10.13111/2066-8201.2019.11.3.16.
- [29] Jieru Fan, Dongguang Li, and Rupeng Li. Evaluation of mav/uav collaborative combat capability based on network structure. *International Journal of Aerospace Engineering*, 2018, 2018. ISSN 16875974. doi: 10.1155/2018/5301752.
- [30] K. P. Valavanis and M. Kontitsis. A historical perspective on unmanned aerial vehicles. *Advances in Unmanned Aerial Vehicles*, pages 15–46, 2 2007. doi: 10.1007/978-1-4020-6114-1_2. URL https://link.springer.com/chapter/10.1007/978-1-4020-6114-1_2.
- [31] Morris Stephen J and Holden Michael. Design of micro air vehicles and flight test validation, 022. URL <https://citeseervx.ist.psu.edu/viewdoc/download?doi=10.1.1.549.7021&rep=rep1&type=pdf>.

References

- [32] Bret Stanford, Peter Ifju, Roberto Albertani, and Wei Shyy. Fixed membrane wings for micro air vehicles: Experimental characterization, numerical modeling, and tailoring. *Progress in Aerospace Sciences*, 44:258–294, 5 2008. ISSN 0376-0421. doi: 10.1016/J.PAEROSCI.2008.03.001.
- [33] M. Lasek, J. Pietrucha, M. Złocka, and K. Sibilski. Analogies between rotary and flapping wings from control theory point of view. *AIAA Atmospheric Flight Mechanics Conference and Exhibit*, 2001. doi: 10.2514/6.2001-4002. URL <https://arc.aiaa.org/doi/abs/10.2514/6.2001-4002>.
- [34] Max F. Platzer, Kevin D. Jones, John Young, and Joseph C.S. Lai. Flapping wing aerodynamics: Progress and challenges. <https://doi.org/10.2514/1.29263>, 46:2136–2149, 5 2012. ISSN 00011452. doi: 10.2514/1.29263. URL <https://arc.aiaa.org/doi/abs/10.2514/1.29263>.
- [35] Krzysztof Sibilski, Mirosław Nowakowski, Dariusz Rykaczewski, Paweł Szczepaniak, Andrzej Zyluk, Anna Sibilska-Mroziewicz, Michał Garbowski, and Wiesław Wróblewski. Identification of fixed-wing micro aerial vehicle aerodynamic derivatives from dynamic water tunnel tests. *Aerospace 2020, Vol. 7, Page 116*, 7:116, 8 2020. ISSN 2226-4310. doi: 10.3390/AEROSPACE7080116. URL <https://www.mdpi.com/2226-4310/7/8/116> <https://www.mdpi.com/2226-4310/7/8/116>.
- [36] S Duranti, Gianpaolo Conte, Denise Lundstrom, Piotr Rudol, Mariusz Wzorek, and Patrick Doherty. Linkmav, a prototype rotary wing micro aerial vehicle, 2007. URL https://www.researchgate.net/figure/The-LinkMAV-rotary-wing-micro-aerial-vehicle_fig1_229091557.
- [37] Kevin D. Jones and Max F. Platzer. Flapping-wing propelled micro air vehicles. *Handbook of Unmanned Aerial Vehicles*, pages 1359–1383, 2015. doi: 10.1007/978-90-481-9707-1_11. URL https://link.springer.com/referenceworkentry/10.1007/978-90-481-9707-1_11.
- [38] Thomas A. Ward, Christopher J. Fearday, Erfan Salami, and Norhayati Binti Soin. A bibliometric review of progress in micro air vehicle research:. <http://dx.doi.org/10.1177/1756829316670671>, 9:146–165, 2 2017. ISSN 17568307. doi: 10.1177/1756829316670671. URL <https://journals.sagepub.com/doi/10.1177/1756829316670671>.
- [39] K. Amadori, D. Lundström, and P. Krus. Automated design and fabrication of micro-air vehicles. *Proceedings of the Institution of Mechanical Engineers, Part G: Journal of Aerospace Engineering*, 226:1271–1282, 10 2012. ISSN 09544100. doi: 10.1177/0954410011419612.
- [40] R. Vijayanandh, M. Senthil Kumar, K. Naveenkumar, G. Raj Kumar, and R. Naveen Kumar. Design optimization of advanced multi-rotor unmanned

References

- aircraft system using fsi. *Lecture Notes in Mechanical Engineering*, pages 299–310, 2019. ISSN 21954364. doi: 10.1007/978-981-13-2718-6_28. URL https://link.springer.com/chapter/10.1007/978-981-13-2718-6_28.
- [41] M Radmanesh, O Nematollahi, M Nili-Ahmadabadi, and M Hassanalian. A novel strategy for designing and manufacturing a fixed wing mav for the purpose of increasing maneuverability and stability in longitudinal axis. *Journal of Applied Fluid Mechanics*, 7:435–446, 2014. ISSN 1735-3645. URL www.SID.ir.
 - [42] A. Aboelezz, M. Hassanalian, A. Desoki, B. Elhadidi, and G. El-Bayoumi. Design, experimental investigation, and nonlinear flight dynamics with atmospheric disturbances of a fixed-wing micro air vehicle. *Aerospace Science and Technology*, 97:105636, 2 2020. ISSN 1270-9638. doi: 10.1016/J.AST.2019.105636.
 - [43] A. Aboelezz, O. Mohamady, M. Hassanalian, and B. Elhadidi. Nonlinear flight dynamics and control of a fixed-wing micro air vehicle: Numerical, system identification and experimental investigations. *Journal of Intelligent & Robotic Systems 2021 101:3*, 101:1–18, 3 2021. ISSN 1573-0409. doi: 10.1007/S10846-021-01352-Y. URL <https://link.springer.com/article/10.1007/s10846-021-01352-y>.
 - [44] Kozera Cyprian Aleksander. Military use of unmanned aerial vehicles – a historical study. *Safety & Defense*, 4:17–21, 10 2018. ISSN 2450-551X. doi: 10.37105/SD.4. URL <https://www.sd-magazine.eu/index.php/sd/article/view/4>.
 - [45] Kenzo NONAMI. Prospect and recent research & development for civil use autonomous unmanned aircraft as uav and mav. *Journal of System Design and Dynamics*, 1:120–128, 2007. doi: 10.1299/JSSD.1.120.
 - [46] Inevitable bedfellows? cooperation on military technology for the development of uavs and cruise missiles in the asia-pacific | policy commons, 2022. URL <https://policycommons.net/artifacts/1427001/inevitable-bedfellow-s-cooperation-on-military-technology-for-the-development-of-uav-s-and-cruise-missiles-in-the-asia-pacific/2041606/>.
 - [47] William W. Greenwood, Jerome P. Lynch, and Dimitrios Zekkos. Applications of uavs in civil infrastructure. *Journal of Infrastructure Systems*, 25:04019002, 1 2019. ISSN 1076-0342. doi: 10.1061/(ASCE)IS.1943-555X.0000464. URL <https://ascelibrary.org/doi/abs/10.1061/%28ASCE%29IS.1943-555X.0000464>.
 - [48] Kadambay Saytov, Nuriddin Abdujabarov, Takhirov Jonibek, Kadambay Saytov, and Saidbek Bobomurodov. Prospects of the development of unmanned aerial vehicles (uavs). *PROSPECTS OF THE DEVELOPMENT OF UNMANNED AERIAL VEHICLES (UAVs)*, 4, 2020. doi: 10.51346/tstu-01.20.3-77-0069. URL <https://www.researchgate.net/publication/345306836>.

References

- [49] Kimon P Valavanis. Advances in unmanned aerial vehicles. *Advances in Unmanned Aerial Vehicles*, 2007. doi: 10.1007/978-1-4020-6114-1.
- [50] Kendra L.B. Cook. The silent force multiplier: The history and role of uavs in warfare. *IEEE Aerospace Conference Proceedings*, 2007. ISSN 1095323X. doi: 10.1109/AERO.2007.352737.
- [51] James H. MacConnell. Ishm & design: A review of the benefits of the ideal ishm system. *IEEE Aerospace Conference Proceedings*, 2007. ISSN 1095323X. doi: 10.1109/AERO.2007.352834.
- [52] Rajesh Kumar. Tactical reconnaissance: Uavs versus manned aircraft, 1997. URL <https://apps.dtic.mil/sti/citations/ADA398405>.
- [53] Matthew Keenon and Joel Grasmeyer. Development of two mavs and vision of the future of mav design. *American Institute of Aeronautics and Astronautics AIAA International Air and Space Symposium and Exposition: The Next 100 Years - Dayton, Ohio (14 July 2003 - 17 July 2003)*, 7 2003. doi: 10.2514/6.2003-2901. URL <https://arc.aiaa.org/doi/pdf/10.2514/6.2003-2901>.
- [54] Abayomi O Agbeyangi, Joseph O Odiete, and Adam B Olorunlomerue. Review on uavs used for aerial surveillance development of an english to yoruba language numeral translation system view project wireless sensor network for potentially harmful gasses view project review on uavs used for aerial surveillance. *Journal of Multidisciplinary Engineering Science and Technology (JMEST)*, 3:2458–9403, 2016. URL <https://www.researchgate.net/publication/309585222>.
- [55] Ovidiu Crivoi, Ioan Doroftei, and Florentina Adascalitei. A survey on unmanned aerial vehicles based on coanda effect. *TEHNOMUS - New Technologies and Products in Machine Manufacturing Technologies*, 2013.
- [56] Derek J Snyder. Design requirements for weaponizing man-portable uas in support of counter-sniper operations, 2011. URL <https://apps.dtic.mil/sti/citations/ADA551913>.
- [57] Xiaohui Wang, Zhen Huang, Guangzhou Sui, and Haishan Lian. Analysis on the development trend of future uav equipment technology. *Academic Journal of Engineering and Technology Science*, 2:114–121, 4 2019. doi: 10.25236/AJETS.020022. URL <https://francis-press.com/papers/337https://francis-press.com/papers/337#abstract>.
- [58] Rui Yin, Wei Li, Zhi Qiang Wang, and Xin Xin Xu. The application of artificial intelligence technology in uav. *Proceedings - 2020 5th International Conference on Information Science, Computer Technology and Transportation, ISCTT 2020*, pages 238–241, 11 2020. doi: 10.1109/ISCTT51595.2020.00048.

References

- [59] James Jackson, Gary Ellingson, and Tim McLain. Rosflight: A lightweight, inexpensive mav research and development tool. *2016 International Conference on Unmanned Aircraft Systems, ICUAS 2016*, pages 758–762, 6 2016. doi: 10.1109/ICUAS.2016.7502584.
- [60] M V Peppa, J Hall, J Goodyear, and J P Mills. Photogrammetric assessment and comparison of dji phantom 4 pro and phantom 4 rtk small unmanned aircraft systems. *School of Engineering, Newcastle University*, 2019. doi: 10.5194/isprs-archives-XLII-2-W13-503-2019. URL <https://doi.org/10.5194/isprs-archives-XLII-2-W13-503-2019>.
- [61] Murat Bronz, Jean Marc Moschetta, Pascal Brisset, and Michel Gorraz. Towards a long endurance mav:. <http://dx.doi.org/10.1260/175682909790291483>, 1: 241–254, 12 2009. ISSN 1756-8293. doi: 10.1260/175682909790291483. URL <https://journals.sagepub.com/doi/abs/10.1260/175682909790291483>.
- [62] M. HASSANALIAN, R. SALAZAR, and A. ABDELKEFI. Conceptual design and optimization of a tilt-rotor micro air vehicle. *Chinese Journal of Aeronautics*, 32:369–381, 2 2019. ISSN 10009361. doi: 10.1016/J.CJA.2018.10.006.
- [63] C. A. Paulson, A. Sóbester, and J. P. Scanlan. The rapid development of bespoke small unmanned aircraft: A proposed design loop. *The Aeronautical Journal*, 121:1683–1710, 11 2017. ISSN 0001-9240. doi: 10.1017/AER.2017.99. URL <https://www.cambridge.org/core/journals/aeronautical-journal/article/rapid-development-of-bespoke-small-unmanned-aircraft/C25DBFCCD9630D2A3281708865E2C6CA>.
- [64] K. Harikumar, Jinraj V. Pushpangathan, and Suresh Sundaram. Effects of propeller flow on the longitudinal and lateral dynamics and model couplings of a fixed-wing micro air vehicle. *Proceedings of the Institution of Mechanical Engineers, Part G: Journal of Aerospace Engineering*, 235, 2021. ISSN 20413025. doi: 10.1177/0954410020966155.
- [65] Kwanchai Chinwicharnam, David Ariza, Jean Marc Moschetta, and Chinnapat Thipyopas. Propeller interaction. In *Aerodynamic characteristics of a low aspect ratio wing and propeller interaction for a tilt-body MAV*, volume 5, 2013. doi: 10.1260/1756-8293.5.4.245.
- [66] Taimur Ali Shams, Syed Irtiza Ali Shah, Ali Javed, and Syed Hossein Raza Hamdani. Airfoil selection procedure, wind tunnel experimentation and implementation of 6dof modeling on a flyingwing micro aerial vehicle. *Micromachines*, 11, 2020. ISSN 2072666X. doi: 10.3390/MI11060553.
- [67] Arivoli Durai. Experimental investigation of lift and drag characteristics of a typical mav under propeller induced flow:.

References

- http://dx.doi.org/10.1260/1756-8293.6.1.63*, 6:63–72, 3 2014. ISSN 17568293.
doi: 10.1260/1756-8293.6.1.63. URL
<https://journals.sagepub.com/doi/abs/10.1260/1756-8293.6.1.63>.
- [68] Taimur Ali Shams, Syed Irtiza Ali Shah, Aamer Shahzad, Ali Javed, and Kashif Mehmod. Experimental investigation of propeller induced flow on flying wing micro aerial vehicle for improved 6dof modeling. *IEEE Access*, 8, 2020. ISSN 21693536. doi: 10.1109/ACCESS.2020.3026005.
- [69] Z Chen and F Yang. Propeller slipstream effect on aerodynamic characteristics of micro air vehicle at low reynolds number. *Appl. Sci.* 2022, 12:4092, 2022. doi: 10.3390/app12084092.
- [70] A Abdul Huq, R Anand Sankar, C Lakshmanan, C Rukesh, D S Kulkarni, M B Subramanya, and B N Rajani. Numerical prediction of aerofoil aerodynamics at low reynolds number for mav application. *Computational & Theoretical Fluid Dynamics Division National Aerospace Laboratories*, 2009.
- [71] H. Liu and H. Aono. Size effects on insect hovering aerodynamics: an integrated computational study. *Bioinspiration & Biomimetics*, 4:015002, 3 2009. ISSN 1748-3190. doi: 10.1088/1748-3182/4/1/015002. URL <https://iopscience.iop.org/article/10.1088/1748-3182/4/1/015002>
<https://iopscience.iop.org/article/10.1088/1748-3182/4/1/015002/meta>.
- [72] W. Null, A. Noseck, and S. Shkarayev. Effects of propulsive-induced flow on the aerodynamics of micro air vehicles. *Collection of Technical Papers - AIAA Applied Aerodynamics Conference*, 1:198–216, 2005. ISSN 10485953. doi: 10.2514/6.2005-4616. URL
<https://arc.aiaa.org/doi/abs/10.2514/6.2005-4616>.
- [73] Phillip M. Munday, Kunihiko Taira, Tetsuya Suwa, Daiju Numata, and Keisuke Asai. Nonlinear lift on a triangular airfoil in low-reynolds-number compressible flow. *Journal of Aircraft*, 52:924–931, 12 2015. ISSN 15333868. doi: 10.2514/1.C032983/ASSET/IMAGES/LARGE/FIGURE12.JPG. URL
<https://arc.aiaa.org/doi/full/10.2514/1.C032983>.
- [74] S. S. Bhat, J. Zhao, J. Sheridan, K. Hourigan, and M. C. Thompson. Aspect ratio studies on insect wings. *Physics of Fluids*, 31:121301, 12 2019. ISSN 1070-6631. doi: 10.1063/1.5129191. URL
<https://aip.scitation.org/doi/abs/10.1063/1.5129191>.
- [75] Gabriel E. Torres and Thomas J. Mueller. Low aspect ratio aerodynamics at low reynolds numbers. *https://doi.org/10.2514/1.439*, 42:865–873, 5 2012. ISSN 00011452. doi: 10.2514/1.439. URL
<https://arc.aiaa.org/doi/abs/10.2514/1.439>.

References

- [76] P. Cosyn and J. Vierendeels. Numerical investigation of low-aspect-ratio wings at low reynolds numbers. <https://doi.org/10.2514/1.16991>, 43:713–722, 5 2012. ISSN 15333868. doi: 10.2514/1.16991. URL <https://arc.aiaa.org/doi/abs/10.2514/1.16991>.
- [77] Mueller T. Low reynolds number vehicles, 1985. URL <https://apps.dtic.mil/sti/citations/ADA153233>.
- [78] P. Cosyn and J. Vierendeels. Numerical investigation of low-aspect-ratio wings at low reynolds numbers. *Journal of Aircraft*, 43:713–722, 2006. ISSN 15333868. doi: 10.2514/1.16991.
- [79] Sridhar Ravi. The influence of turbulence on a flat plate aerofoil at reynolds numbers relevant to mavs, 2011. URL <https://researchrepository.rmit.edu.au/esploro/outputs/doctoral/The-influence-of-turbulence-on-a/9921861600501341>.
- [80] Blair Perot and Hudong Wang. Modeling separation and reattachment using the turbulent potential model. *Engineering Turbulence Modelling and Experiments* 4, pages 145–154, 1 1999. doi: 10.1016/B978-008043328-8/50013-8.
- [81] Tai Ran Niew. The stability of the flow in a laminar separation bubble - nasa/ads, 1993. URL <https://ui.adsabs.harvard.edu/abs/1993STIN...9526809N/abstract>.
- [82] Olaf Marxen and Ulrich Rist. Mean flow deformation in a laminar separation bubble: separation and stability characteristics. *Journal of Fluid Mechanics*, 660:37–54, 2010. ISSN 1469-7645. doi: 10.1017/S0022112010001047. URL <https://www.cambridge.org/core/journals/journal-of-fluid-mechanics/article/abs/mean-flow-deformation-in-a-laminar-separation-bubble-separation-and-stability-characteristics/C807513D042579713DC18F9B70CB2366>.
- [83] Peter Crimi and Barry L Reeves. Analysis of leading-edge separation bubbles on airfoils. *AIAA JOURNAL*, 14, 1976. doi: 10.2514/3.7250. URL <http://arc.aiaa.org>.
- [84] John H McMaster. The flight of the bumblebee and related myths of entomological engineering: Bees help bridge the gap between science and engineering on jstor, 1989. URL <https://www.jstor.org/stable/27855657?seq=1>.
- [85] Bruno A. Roccia, Sergio Preidikman, Marcos L. Verstraete, and Dean T. Mook. Influence of spanwise twisting and bending on lift generation in mav-like flapping wings. *Journal of Aerospace Engineering*, 30:04016079, 8 2016. ISSN 0893-1321. doi: 10.1061/(ASCE)AS.1943-5525.0000677. URL [https://ascelibrary.org/doi/10.1061/\(ASCE\)AS.1943-5525.0000677](https://ascelibrary.org/doi/10.1061/(ASCE)AS.1943-5525.0000677).

References

- brary.org/doi/abs/10.1061/%28ASCE%29AS.1943-5525.0000677https://ascelibrary.org/doi/full/10.1061/%28ASCE%29AS.1943-5525.0000677.
- [86] H. Winter. Flow phenomena on plates and airfoils of short span - unt digital library, 1936. URL <https://digital.library.unt.edu/ark:/67531/metadc63411/>.
- [87] Suyang Qin, Zifeng Weng, Zhuoqi Li, Yang Xiang, and Hong Liu. On the controlled evolution for wingtip vortices of a flapping wing model at bird scale. *Aerospace Science and Technology*, 110:106460, 3 2021. ISSN 1270-9638. doi: 10.1016/J.AST.2020.106460.
- [88] H Zimmerman Langley. Tech caz n0 s national advisory committee for aeronautics aerodynamic characteristics of several airfoils of low aspect ratio. *NATIONAL ADVISORY COMMITTEE FOR AERONAUTICS*, 1936.
- [89] Adam C. DeVoria and Kamran Mohseni. A vortex model for forces and moments on low-aspect-ratio wings in side-slip with experimental validation. *Proceedings of the Royal Society A: Mathematical, Physical and Engineering Sciences*, 473, 2 2017. ISSN 14712946. doi: 10.1098/RSPA.2016.0760. URL <https://royalsocietypublishing.org/doi/10.1098/rspa.2016.0760>.
- [90] Simon Watkins, Juliette Milbank, Benjamin J. Loxton, and William H. Melbourne. Atmospheric winds and their implications for microair vehicles. <https://doi.org/10.2514/1.22670>, 44:2591–2600, 5 2012. ISSN 00011452. doi: 10.2514/1.22670. URL <https://arc.aiaa.org/doi/10.2514/1.22670>.
- [91] Matt Shields and Kamran Mohseni. Inherent stability modes of low-aspect-ratio wings. *Journal of Aircraft*, 52:141–155, 1 2015. ISSN 15333868. doi: 10.2514/1.C032636/ASSET/IMAGES/LARGE/FIGURE13.JPG. URL <https://arc.aiaa.org/doi/10.2514/1.C032636>.
- [92] Thomas J. Mueller and James D. DeLaurier. Aerodynamics of small vehicles. <http://dx.doi.org/10.1146/annurev.fluid.35.101101.161102>, 35:89–111, 11 2003. ISSN 00664189. doi: 10.1146/ANNUREV.FLUID.35.101101.161102. URL <https://www.annualreviews.org/doi/abs/10.1146/annurev.fluid.35.101101.161102>.
- [93] Alain Pelletier and Thomas J. Mueller. Low reynolds number aerodynamics of low-aspect-ratio, thin/flat/cambered-plate wings. <https://doi.org/10.2514/2.2676>, 37:825–832, 5 2012. ISSN 00218669. doi: 10.2514/2.2676. URL <https://arc.aiaa.org/doi/10.2514/2.2676>.
- [94] Prandtl L. Mutual influence of wings and propeller - unt digital library, 1921. URL <https://digital.library.unt.edu/ark:/67531/metadc53773/>.

References

- [95] Luis R. Miranda and James E. Brennan. Aerodynamic effects of wingtip-mounted propellers and turbines. *AIAA Paper*, pages 221–228, 1986. ISSN 01463705. doi: 10.2514/6.1986-1802. URL <https://arc.aiaa.org/doi/abs/10.2514/6.1986-1802>.
- [96] Tomas Sinnige, Nando Van Arnhem, Tom C.A. Stokkermans, Georg Eitelberg, and Leo L.M. Veldhuis. Wingtip-mounted propellers: Aerodynamic analysis of interaction effects and comparison with conventional layout. *Journal of Aircraft*, 56:295–312, 2019. ISSN 15333868. doi: 10.2514/1.C034978.
- [97] L. L.M. Veldhuis and P. M. Heyma. Aerodynamic optimisation of wings in multi-engined tractor propeller arrangements. *Aircraft Design*, 3:129–149, 9 2000. ISSN 1369-8869. doi: 10.1016/S1369-8869(00)00010-0.
- [98] L Veldhuis. Review of propeller-wing aerodynamic interference, 2004. URL http://icas.org/ICAS_ARCHIVE/ICAS2004/PAPERS/065.PDF.
- [99] M. H. Rizk. Propeller in slipstream/wing interaction in the transonic regime. <https://doi.org/10.2514/3.57482>, 18:184–191, 5 2012. ISSN 00218669. doi: 10.2514/3.57482. URL <https://arc.aiaa.org/doi/abs/10.2514/3.57482>.
- [100] L Prandtl. Mutual influence of wings and propeller, 1931. URL <https://ntrs.nasa.gov/api/citations/19930080882/downloads/19930080882.pdf>.
- [101] A Franke and F Weinig. The effect of the slipstream on an airplane wing - nasa technical reports server (ntrs), 1939. URL <https://ntrs.nasa.gov/citations/19930094496>.
- [102] Antony Jameson. (pdf) analysis of wing slipstream flow interaction, 1970. URL https://www.researchgate.net/publication/24381872_Analysis_of_wing_slipstream_flow_interaction.
- [103] N Ellis. Aerodynamics of wing-slipstream interaction: a numerical study,, 1971. URL <https://apps.dtic.mil/sti/citations/AD0743257>.
- [104] Leo Veldhuis, Tom Stokkermans, Tomas Sinnige, and Georg Eitelberg. Analysis of swirl recovery vanes for increased propulsive efficiency in tractor propeller aircraft. *30th Congress of the International Council of the Aeronautical Sciences*. 60., 2016.
- [105] Jieliang Shen, Yan Su, Qing Liang, and Xinhua Zhu. Calculation and identification of the aerodynamic parameters for small-scaled fixed-wing uavs. *Sensors 2018, Vol. 18, Page 206*, 18:206, 1 2018. ISSN 1424-8220. doi: 10.3390/S18010206. URL <https://www.mdpi.com/1424-8220/18/1/206/htmhttps://www.mdpi.com/1424-8220/18/1/206>.

References

- [106] Brian Roberts, Rick Lind, and Mrinal Kumar. Polynomial chaos analysis of mav's in turbulence. *AIAA Atmospheric Flight Mechanics Conference 2011*, 2011. doi: 10.2514/6.2011-6214.
- [107] Pijush Kanti Kundu David R. Dowling, Ira Cohen. Aerodynamics. *Fluid Mechanics*, pages 691–728, 1 2012. doi: 10.1016/B978-0-12-382100-3.10014-9. URL <https://linkinghub.elsevier.com/retrieve/pii/B9780123821003100149>.
- [108] PM Hrad. Conceptual design tool for fuel-cell powered micro air vehicles. *Defense Technical Information Center*, 2010. URL <https://apps.dtic.mil/sti/citations/ADA517534>.
- [109] Kai Zhang, Bharg Shah, and Onur Bilgen. Low-reynolds-number aerodynamic characteristics of airfoils with piezocomposite trailing surfaces. *AIAA Journal*, 60:2701–2706, 4 2022. ISSN 0001-1452. doi: 10.2514/1.J061214/ASSET/IMAGES/LARGE/FIGURE6.JPG. URL <https://arc.aiaa.org/doi/full/10.2514/1.J061214>.
- [110] William Bollay. A non-linear wing theory and its application to rectangular wings of small aspect ratio. *ZAMM - Journal of Applied Mathematics and Mechanics / Zeitschrift für Angewandte Mathematik und Mechanik*, 19:21–35, 1 1939. ISSN 1521-4001. doi: 10.1002/ZAMM.19390190103. URL <https://onlinelibrary.wiley.com/doi/full/10.1002/zamm.19390190103><https://onlinelibrary.wiley.com/doi/abs/10.1002/zamm.19390190103><https://onlinelibrary.wiley.com/doi/10.1002/zamm.19390190103>.
- [111] S. M. Belotserkovskii. Calculation of the flow around wings of arbitrary planform over a wide range of angles of attack. *Fluid Dynamics 1972 3:4*, 3: 20–27, 7 1968. ISSN 1573-8507. doi: 10.1007/BF01019187. URL <https://link.springer.com/article/10.1007/BF01019187>.
- [112] Victor Gomez, Nicolas Gomez, Jorge Rodas, Enrique Paiva, Maarouf Saad, and Raul Gregor. Pareto optimal pid tuning for px4-based unmanned aerial vehicles by using a multi-objective particle swarm optimization algorithm. *Aerospace 2020, Vol. 7, Page 71*, 7:71, 6 2020. ISSN 2226-4310. doi: 10.3390/AEROSPACE7060071. URL <https://www.mdpi.com/2226-4310/7/6/71/htm><https://www.mdpi.com/2226-4310/7/6/71>.
- [113] Abdelwahid Boutemedjet, Marija Samardžić, Lamine Rebhi, Zoran Rajić, and Takieddine Mouada. Uav aerodynamic design involving genetic algorithm and artificial neural network for wing preliminary computation. *Aerospace Science and Technology*, 84:464–483, 1 2019. ISSN 1270-9638. doi: 10.1016/J.AST.2018.09.043.

References

- [114] José Rivera Parga, Mark F. Reeder, Troy Leveron, and Ken Blackburn. Experimental study of a micro air vehicle with a rotatable tail. *Journal of Aircraft*, 44, 2007. ISSN 15333868. doi: 10.2514/1.24192.
- [115] Shuvrangshu Jana, Harikumar Kandath, Mayur Shewale, and M. Seetharama Bhat. Effect of propeller-induced flow on the performance of biplane micro air vehicle dynamics. *Proceedings of the Institution of Mechanical Engineers, Part G: Journal of Aerospace Engineering*, 234:716–728, 3 2020. ISSN 20413025. doi: 10.1177/0954410019883097.

Appendix A

Work Health and Safety

Ensuring that a safe work environment is present for everyone is critical to reducing injury and illness and increases productivity. In order to do this it is a requirement of the Australian Work, Health and Safety laws to do the following[]: _____

cite

- Provide a safe work environment
- Provide and maintain safe machinery and structures
- Provide safe ways of working
- Ensure safe use, handling and storage of machinery, structures and substances
- Provide and maintain adequate facilities
- Provide any information, training, instruction or supervision needed for safety
- Monitor the health of workers and conditions at the workplace.

Workers also have several obligations to both themselves and those around them. They must[]:

- Take care of their own health and safety
- Take care not to do anything that could hurt others

Work Health and Safety

- Follow WHS instructions
- Follow the workplace's WHS policies and procedures

This section analyses the significant health and safety concerns in regards to the development, collation of data and writing of this thesis. The main topics covered are physical health, mental health and wind tunnel safety.

		Impact →				
		Negligible	Minor	Moderate	Significant	Severe
↑ Likelihood	Very Likely	Low Med	Medium	Med Hi	High	High
	Likely	Low	Low Med	Medium	Med Hi	High
	Possible	Low	Low Med	Medium	Med Hi	Med Hi
	Unlikely	Low	Low Med	Low Med	Medium	Med Hi
	Very Unlikely	Low	Low	Low Med	Medium	Medium

Fig. A.1 Risk matrix. From <https://www.armsreliability.com/page/resources/blog/beyond-the-risk-matrix>.

A.1 Physical Health

This thesis involved long hours of repetitive desk tasks. These tasks done over long durations led to bad posture, wrist strain, eye strain

In a standard office, work is often long, repetitive, and stationary. Bad posture, uncomfortable chairs, mispositioned monitors, wrist strain over cramped keyboards,

A.1 Physical Health

poor lighting or glare are just a few of the most common risks and hazards to physical health.

At Accenture and home, the following precautions were observed:

1. Education on the proper position to work in was studied from A.2. Notably, the height of the chair is set to the appropriate height to allow feet to rest in an almost 90 deg angle, the top of the monitor edge at eye level, and the monitor slightly tilted up to equalise the distance to all corners of the screen.
2. Good chairs were selected. I purchased a Herman Miller Aeron chair for work at home, known for its world-renowned ergonomics.
3. Used a second external monitor to relieve neck strain, as it is possible to adjust the monitor's position to the optimal position. This also provided a significant productivity boost. The brightness was also adequately adjusted to bring the most comfort to the eyes.
4. A standing desk was purchased for working at home.
5. Regular breaks were taken with the team during the time at the office.
6. An ergonomic keyboard, the Kinesis Advantage 2, was used to relieve wrist strain and improve productivity with the features such as macros.

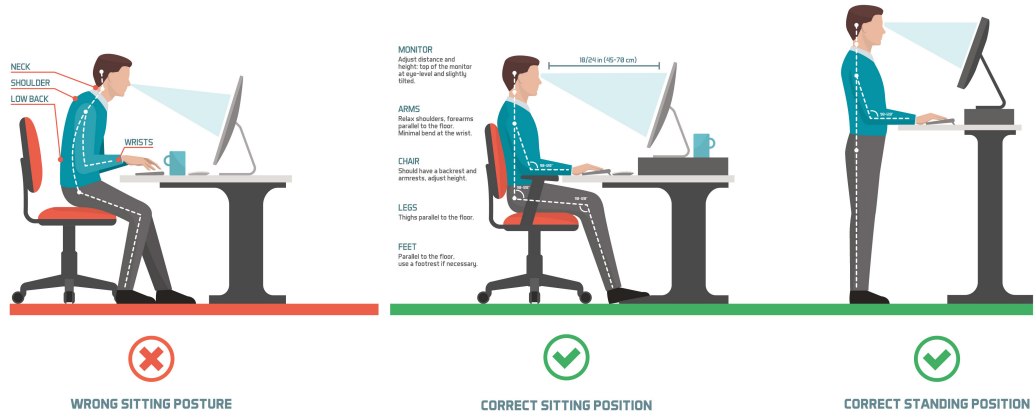


Fig. A.2 Best posture at a desk. From: <https://healthandbalance.com.au/workstation-desk-posture-ergonomics/>

Although there are many sources of long-term physical issues, these can be easily managed with awareness and mitigated effectively, resulting in a low level of risk.

A.2 Covid-19 precautions

Covid-19 has undeniably impacted the world in many ways. This highly infectious disease caused major lockdowns and shifted work from the office to the home for extended periods. In order to follow national and state requirements, Accenture and employees worked remotely and suspended office visits. Return to the office was first announced in mid-November, where a number of precautions were followed:

1. All state and national requirements were followed, including masks in public indoor areas and on transport, QR code check-ins in all locations required, and mandatory bookings for visits to the office.
2. Social distancing in all public areas.

3. Sanitising hands on every entry to the office.
4. Disallowing guest visits to the office.

Although the severity of symptoms one suffers from contracting Covid-19 vary wildly in the younger age group, the potential to be sick for a week or more, in addition to the mandatory self-isolation period, is highly disruptive to work and the greater population. As such, the threat of Covid-19 results in high risk.

A.3 Mental health

Mental health is an often under-looked part of one's health. It varies greatly from person to person, and many factors play into one's overall mental health, including social health, work-life balance, and financial status. Without careful consideration, planning and awareness of one's mental health, the employee's productivity may drop sharply.

A number of precautions were taken to care for my mental health:

1. Ensuring I was enjoying the work I was doing. I transferred internally between teams to find more exciting work that I could grow and learn in while also finding a more relevant thesis topic aligned with my interests.
2. Coming into the office when practical. Although there were many days where I was the only team member in the office, being able to experience the office, grab hot drinks in the morning with colleagues, and work in an environment separate from home was very beneficial.
3. Preventing work hours from extending into my personal time too often.

Work Health and Safety

Mental health is a complex risk to quantify since it is difficult to measure and includes many factors. Overall the onus is mainly on the employee to ensure they take the proper precautions and use the available resources such as sick leave or personal time off. Particularly with the challenging program that is ESIPS, this risk is categorised as a moderate risk.